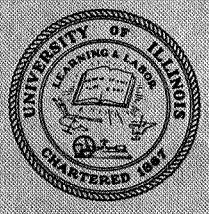

UNIVERSITY OF ILLINOIS
URBANA

AERONOMY REPORT NO. 27

STUDIES OF LOWER IONOSPHERE DRIFTS BY THE THREE-RECEIVER TECHNIQUE

by

D. Guha

August 15, 1968

NGR-14-005-013
Supported by
National Aeronautics and Space Administration
Grant (NsG-511)

Aeronomy Laboratory
Department of Electrical Engineering
University of Illinois
Urbana, Illinois

CITATION POLICY

The material contained in this report is preliminary information circulated rapidly in the interest of prompt interchange of scientific information and may be later revised on publication in accepted aeronomic journals. It would therefore be appreciated if persons wishing to cite work contained herein would first contact the authors to ascertain if the relevant material is part of a paper published or in process.

A E R O N O M Y R E P O R T

N O. 2 7

STUDIES OF LOWER IONOSPHERE DRIFTS BY THE THREE-RECEIVER TECHNIQUE

by

D. Guha

August 15, 1968

Supported by
National Aeronautics and
Space Administration
NsG-511

Aeronomy Laboratory
Department of Electrical Engineering
University of Illinois
Urbana, Illinois

ABSTRACT

This paper describes a simple method for determining the ionospheric drifts by the three-receiver technique.

A description is given of the equipment which was used for measurements.

The results of measurements taken at the Field Station of the Aeronomy Laboratory during the summer months in 1967 are presented.

ACKNOWLEDGEMENTS

I want to thank Prof. S. A. Bowhill and Dr. J. S. Shirke for their constant guidance throughout the course of this research work. Thanks are due to G. W. Henry, Jr. and his group in the Aeronomy Laboratory who have developed the instrument.

The work described in this report was supported by the National Aeronautics and Space Administration under grant NsG-511.

TABLE OF CONTENTS

Page

ABSTRACT ii

ACKNOWLEDGEMENTS iii

LIST OF FIGURES vi

1. STUDIES OF LOWER IONOSPHERE DRIFTS BY THE THREE-RECEIVER TECHNIQUE . . . 1

1.1 Introduction 1

1.2 Previous Methods 1

2. DESCRIPTION OF THE EQUIPMENT 5

2.1 50 kw Pulse Transmitter 5

2.1.1 Tunable Pulsed Oscillator Unit 5
2.1.2 Excitor and Pulse Modulator Unit 8
2.1.3 Driver Amplifier Stage 10
2.1.4 Final Amplifier Unit 12

2.2 Switched Preamplifier Chain 14

2.3 Pulse Receiver 16

2.3.1 RF Amplifier, Mixer and Local Oscillator Unit 18
2.3.2 IF Amplifier, Detector and DC Amplifier Unit 21

2.4 Antennas 27

2.5 Camera and Time Marker System 27

3. METHODS OF ANALYSIS 31

3.1 Definitions and Basic Equations 31

3.1.1 Correlation Functions 31

3.2 Velocities 33

3.2.1 V', Ficitious Drift Velocity 34
3.2.2 V_D, Steady Drift Velocity 34
3.2.3 V_R Short Period Random Velocity 34
3.2.4 V'_R Fading Velocity 34

3.3 Methods of Measuring τ_o and τ_s Assuming Gaussian Distribution . . . 35

TABLE OF CONTENTS (continued)

Page

3.4 Spatial Correlation Ellipse and Structure Size. 38

3.5 Anisotropy Corrections. 43

3.6 Sampling Theory and Determination of Sampling Interval. 44

4. EXPERIMENTAL RESULTS 49

4.1 Drift Velocities. 49

4.2 Velocities. 60

4.3 Spatial Properties of Diffraction Pattern 60

4.4 Semidiurnal Components. 70

5. SUMMARY AND CONCLUSION 74

REFERENCES 76

LIST OF FIGURES

Figure		Page
2.1	Block diagram of drifts experiment	6
2.2	Block diagram of the transmitter (after Henry 1966)	7
2.3	Pulsed oscillator unit (after Henry 1966)	9
2.4	Excitor and pulse modulator (after Henry 1966)	11
2.5	Driver amplifier (after Henry 1966)	13
2.6	Improved final amplifier (after Henry 1966)	15
2.7	Electronically switched preamplifiers	17
2.8	RF stages of the receiver (after Henry 1966)	22
2.9	IF detector and DC amplifier (after Henry 1966)	24
2.10	Receiver pulse response (after Henry 1966)	25
2.11	Receiving antenna arrangement	28
2.12	Transmitting antenna arrangement	29
3.1	Typical auto- and cross-correlograms	32
3.2	Spatial correlation ellipse in the receiver triangle	42
3.3	Auto-correlograms for different sampling intervals	48
4.1	Hourly variation of drift velocity, May 4, 1967	52
4.2	Hourly variation of drift velocity, May 19, 1967	53
4.3	Hourly variation of drift velocity, June 9, 1967	54
4.4	Hourly variation of drift velocity, June 20, 1967	55
4.5	Hourly variation of N-S and E-W component of drift velocity, May 4, 1967	56
4.6	Hourly variation of N-S and E-W component of drift velocity, May 19, 1967	57

LIST OF FIGURES (Continued)

Figure		Page
4.7	Hourly variation of N-S and E-W component of drift velocity, June 9, 1967	58
4.8	Hourly variation of N-S and E-W component of drift velocity, June 20, 1967	59
4.9	Distribution of drift velocity, May and June 1967	61
4.10	Distribution of random velocity, May and June 1967	62
4.11	Mean hourly variation of E-W component of drift velocity, May 1967	63
4.12	Mean hourly variation of N-S component of drift velocity, May 1967	64
4.13	Mean hourly variation of E-W component of drift velocity, June 1967	65
4.14	Mean hourly variation of N-S component of drift velocity, June 1967	66
4.15	Distribution of axial ratio S, May and June 1967	67
4.16	Distribution of tilt angle ψ, May and June 1967	68
4.17	Distribution of structure size of the irregularities d, May and June 1967	69
4.18	Polar plot of semidiurnal component of drift velocity, May 1967	71
4.19	Polar plot of semidiurnal component of drift velocity, June 1967	72

1. STUDIES OF LOWER IONOSPHERE DRIFTS BY THE THREE-RECEIVER TECHNIQUE

1.1 Introduction

The principal objectives of this study are: (1) to develop theoretically a practical method of determination of ionospheric drift of the ionosphere; (2) application of the above method to evaluate the motion and structure of the irregularities of the E layer.

There are various methods of observing the drift of the irregularities in the ionosphere. Among the radio methods which are widely used is the spaced receiver method for ground-based observation. Various workers have studied the ionospheric drift by the three receiver technique and a short resume of the different methods is presented here first and subsequently the method followed in this study will be described in detail.

1.2 Previous Methods

Mitra (1949) developed the spaced receiver technique using the original ideas of Ratcliffe and Pawsey (1933). The fading records from three spatially separated receivers were compared. He measured the time lag between corresponding maxima on the three records. At any instant of time the pattern of amplitude variations over the ground can be represented by contours of equal amplitude. In general, these contours may take any arbitrary shape determined by the scattering and diffraction of the radio waves by the ionospheric irregularities. The mean change of amplitude, after traveling the fixed distance in a given direction is determined by averaging the measurements on many irregularities. If this average value is independent of direction then the pattern is said to be statistically isotropic. It was assumed in Mitra's method that the

contours of equal amplitude are isotropic in shape. This blob, as it is called, drifts over the triangular arrangement of receivers. If only the time displacement of the maxima are considered, the motion of the blob over the receivers can be replaced by the motion of the line of maxima and hence the drift velocity was determined from the time shift of the maxima observed.

This method is simple to apply and the results may be obtained quickly. There are several difficulties with this approach. Although the pattern is assumed statistically isotropic, the individual contours of constant amplitude may not be circular. Briggs and Page (1954) and Briggs and Spencer (1954) have studied this problem and showed that the line of maxima is not necessarily normal to the drift direction. The variations about this direction are described by a probability distribution. This leads to a variability in time shift, which is not easily handled by the Mitra method.

The assumption is also made in the Mitra analysis that there are no random motions superimposed on the steady drift. This is not always the case, and the effect of random motions should be included in any general method of analysis.

Pütter (1954) described a method for analyzing the fading records, using time lags between corresponding maxima, which was more general than the Mitra method. Pütter considered that the line of maxima makes an angle ψ with the normal to the drift direction and is not necessarily zero as in Mitra's analysis. But this method did not include the effect of random motions superimposed on the steady drift.

Briggs, et al. (1950) gave the general approach of studying the fading record based on correlation methods. Both the steady drift and the superimposed random motions of the interference pattern on the ground were systematically analyzed. The use of correlation functions in this work requires that the time

series be statistically stationary. That is, important statistical parameters, such as mean amplitude and standard deviation, do not vary over the length of time for which the analysis is being carried out. Briggs, et al. (1950) defined four velocities (which will be described in detail in Chapter 3) which can be determined from the correlation functions of the fading records. Their method consists of plotting $(\tau'^2-\tau^2)$ vs τ from the fading records, where τ = time lag associated with the cross-correlation coefficient and τ' = time lag associated with the auto-correlation coefficient. This plot is theoretically a straight line and from intercept and slope of this line, the drift and random velocities are calculated. It has been assumed that the random velocity V_R is isotropically distributed over the ground. The contours of equal amplitude on the ground was assumed to be statistically isotropic and can be represented by a circular pattern. The removal of the restriction of isotropy of the ground pattern was discussed by Phillips and Spencer (1955) and the method has been modified accordingly. The removal of isotropy restriction has been taken care of by correction terms. The methods of Briggs, et al. (1950) and Phillips and Spencer (1955) combined are considered the most general approach so far developed in the analysis of spaced-receiver measurements. They include not only the effects of random change in the form and the anisotropy of the diffraction patterns, but also shed light on the statistical properties of the diffraction patterns such as the structure size, the axial ratio and the tilt angle of the anisotropy ellipse.

However, in actual analysis the plots of $(\tau'^2-\tau^2)$ vs τ as defined in Briggs, et al. (1950) method deviate considerably from straight lines due to sampling errors and the method requires an enormous amount of computational work in determining the best-fit straight line before the velocities can be determined.

For this reason the use of this method was considered impractical in the present work and it was decided to adopt a simpler but not necessarily less accurate method for computing velocities from the correlation functions. This analysis was developed by Lee (1962) and the present analysis is based on his method.

There is no necessity of plotting the Briggs, et al. (1950) straight line. The four velocities are obtained directly from the fading records by assuming Gaussian distribution of the auto- and cross-correlation functions. The anisotropy parameters and the correlation ellipse can be determined directly from the correlation functions determined. The whole program can be fed to the computer and the values of drift velocity, random velocity, axial ratio, tilt angle, etc. all are directly obtained from the fading data of the three receivers.

The work done in this thesis follows closely the Lee's method of analysis and therefore the procedure will be described in detail in Chapter 3. The chapters are arranged as follows: (1) In Chapter 1 different methods of analysis has been compared and the method followed in this analysis is indicated. (2) In Chapter 2 the equipment by which the measurement is done is described. (3) Chapter 3 deals with the methods of analysis followed. (4) Chapter 4 gives the experimental results obtained at the Aeronomy Laboratory of the University of Illinois. (5) In Chapter 5 the summary and conclusion of these results are given.

2. DESCRIPTION OF THE EQUIPMENT

This chapter describes the arrangement of the radio apparatus which were made to observe simultaneous amplitude fading records of the radio signals reflected from the ionosphere at the three spaced receiver sites. The three signals are picked up by vertical loop aerials (1 sq meter area) arranged at the corners of an equilateral triangle spaced 100 meters apart. These signals are fed through switched preamplifier chain and a properly gated receiver to give three fading records simultaneously on the oscilloscope screen at three levels. These are photographed by a slowly moving high sensitive film. A single 50 kw transmitter is used as the common signal source. The operating frequency used is 2.66 MHz. The block diagram of the arrangement is shown in Figure 2.1. The description of the individual units will be given now.

2.1 50 kw Pulse Transmitter

The electrical characteristics are given below:

Power output = 50 kw during pulse

Pulse width = 50 μsec

Pulse repetition rates = 0.5, 1, 2, 5 pps, 5 pps is used for drift measurement

Center frequency = 2.00 to 3.50 MHz, frequency used is 2.66 MHz

Output impedance = 50 ohms balanced.

The block diagram of the transmitter is shown in Figure 2.2.

2.1.1 Tunable Pulsed Oscillator Unit

Single 2N697 transistor in a Hartley oscillator circuit generates a continuous wave signal. Long-term stability of the oscillator stage has been measured to be ± 1 part in 10^4 in the tunable mode and 1 part in 10^5 in a

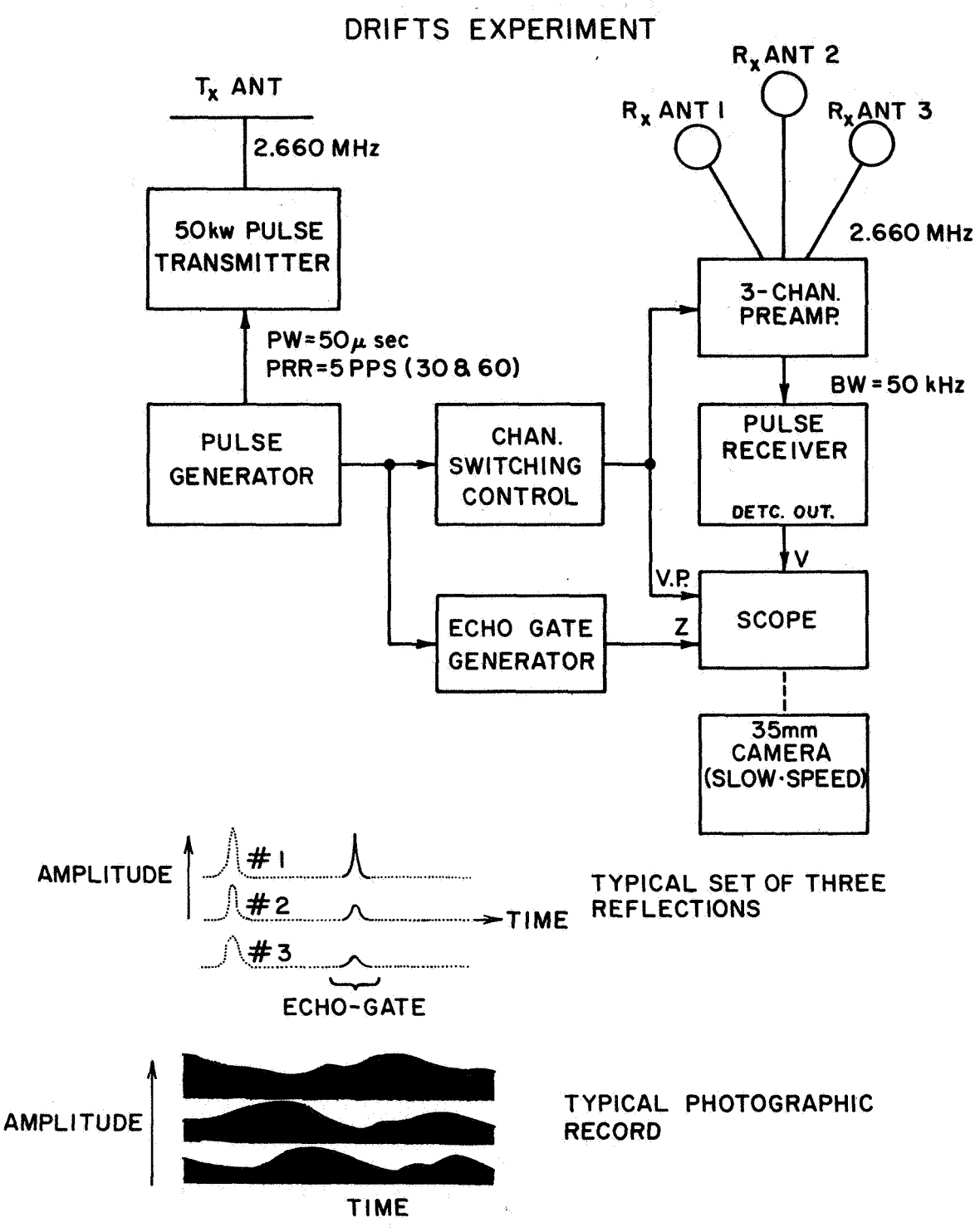

Figure 2.1 Block diagram of drifts experiment.

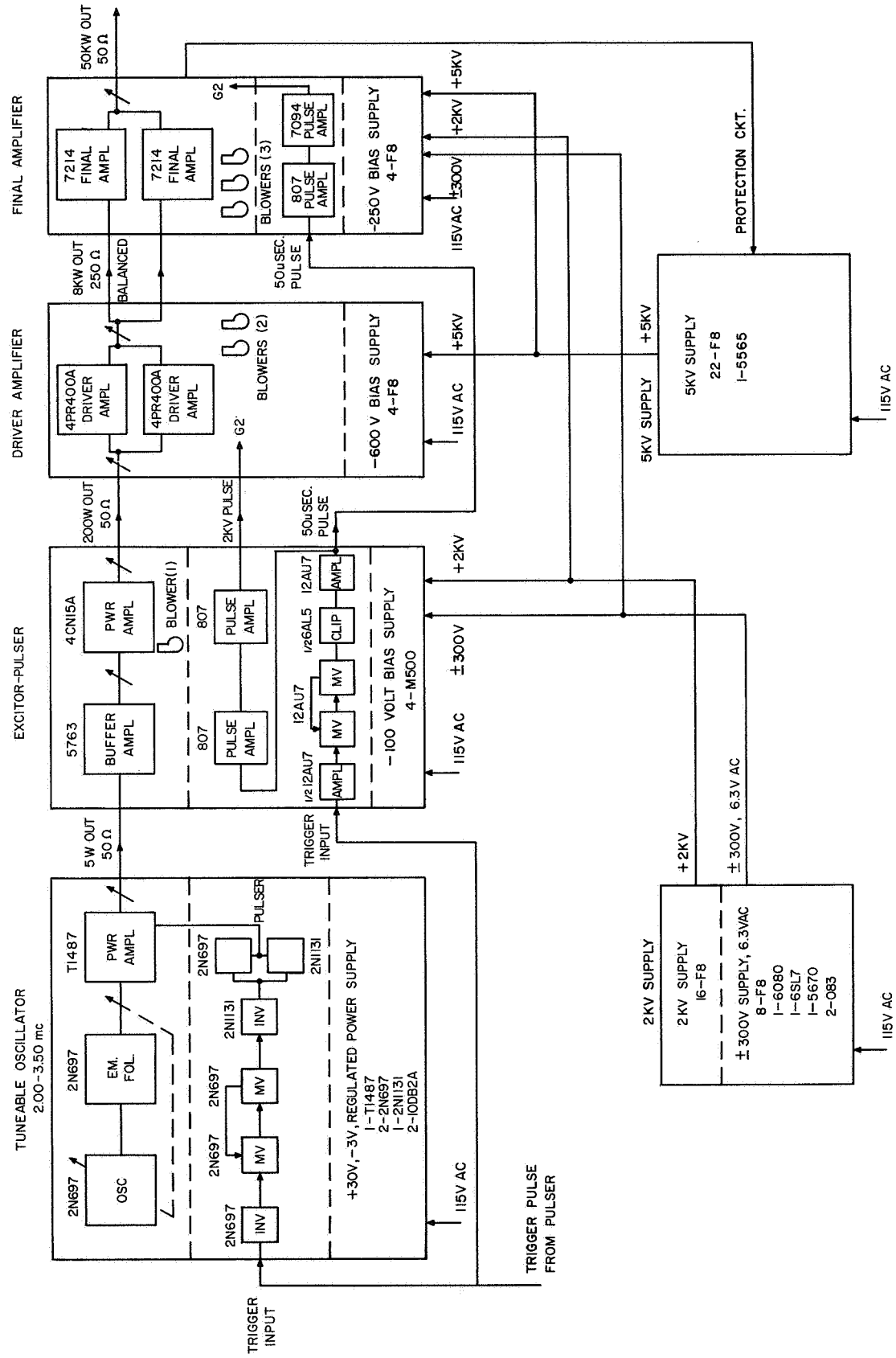

Figure 2.2 Block diagram of the transmitter (after Henry, 1966).

crystal-controlled mode. The oscillator stage is followed by a 2N697 emitter follower buffer amplifier to eliminate frequency instability caused by the variable nature of the pulsed load presented by the pulsed amplifier stage. The pulsed amplifier stage uses one TI487 transistor in a common-emitter base pulsed RF amplifier circuit operating in class B. This stage delivers approximately 5 watts of pulsed RF energy at the operating frequency into a 50 ohm load.

A seven transistor circuit generates the 50 μsec pulse to gate the base of the pulsed amplifier stage. A 2N697 transistor inverts the positive trigger pulse generated by the timing and control unit and triggers a two transistor (2N697) monostable multivibrator circuit that generates a 50 μsec pulse for each trigger pulse. A two stage amplifier incorporating one 2N398A and one 2N697 transistor shapes the pulse and couples it to the two transistor pulse modulator stage (2N697 and 2N1131) which pulse the base of the output amplifier. The circuit diagram is shown in Figure 2.3.

2.1.2 Excitor and Pulse Modulator Unit

It is composed of a 5763 RF amplifier and a 4CN15A power RF amplifier stage that can deliver approximately 150 watts during the pulse to a 50 ohm unbalanced load. Also included in this unit is a pulse generator circuit, and a high voltage pulse modulator circuit.

Output of the pulsed oscillator unit is coupled directly to the gird of a 5763 class C amplifier stage. The output of the 5763 amplifier is controlled by varying the screen voltage.

The excitor power amplifier stage uses one Eimac 4CN15A tube in a tuned RF amplifier circuit. This stage is keyed by a 1 Kv pulse applied to the plate and through a dropping circuit to the screen. The tuned output of the 4CN15A

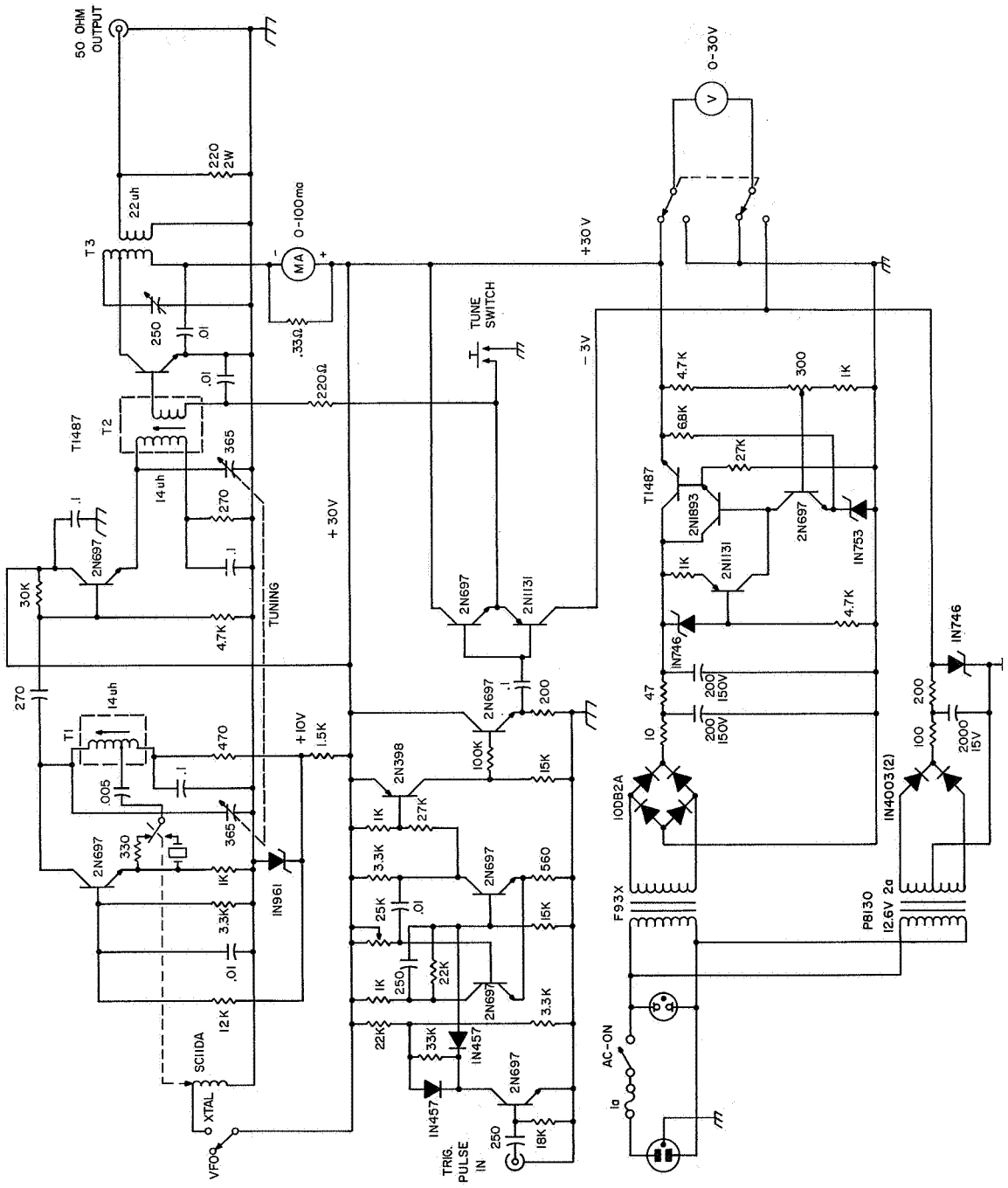

Figure 2.3 Pulsed oscillator unit (after Henry, 1966).

amplifier is coupled to the 50 ohm coaxial cable by means of conventional link coupling.

The trigger pulse generated by the timing and control unit is inverted in a 12AU7 stage and applied to a 12AU7 50 μsec monostable multivibrator. This pulse is shaped and amplified in the following stages of the 6AL5 and 12AU7 tubes. The resultant 60 volt negative pulse gates the pulse modulators for the exciter, driver and final amplifier units of the transmitters. The pulse modulator circuit for the exciter and driver stages uses an 807W/5933 tube as a pulse amplifier and a 3E29 tube as a pulse modulator to provide a +1000 volt pulse for keying of the plate and screen grid circuits of the 4CN15A and the screen-grid circuit of the 4PR400A driver tubes. The output of the pulse modulator is clamped at -300 volts under conditions of no pulse input to assure complete cutoff of the keyed stages. The circuit diagram is given in Figure 2.4.

2.1.3 Driver Amplifier Stage

This is a push-pull class C amplifier capable of delivering approximately 5 kw of RF energy during the pulse to the grids of the final amplifier tubes. Two Eimac 4PR400A tetrods are used in a class C, push-pull amplifier stage. These tubes are designed specifically for use in pulsed service and incorporates larger cathode elements to withstand higher pulse currents than would be expected in cw operation. The 4PR400A tubes easily provide sufficient driving power to the final amplifier without exceeding any other ratings. These tubes are keyed by pulsing the screen supply with the same pulse modulator used to key the 4CN15A stage of the excitor.

An Eimac SK-410 air system socket and chimney is used for each 4PR400A. Separate 15 cfm blowers are used to cool each tube. Since the duty cycle of the transmitter is very low, cooling requirements are minimal.

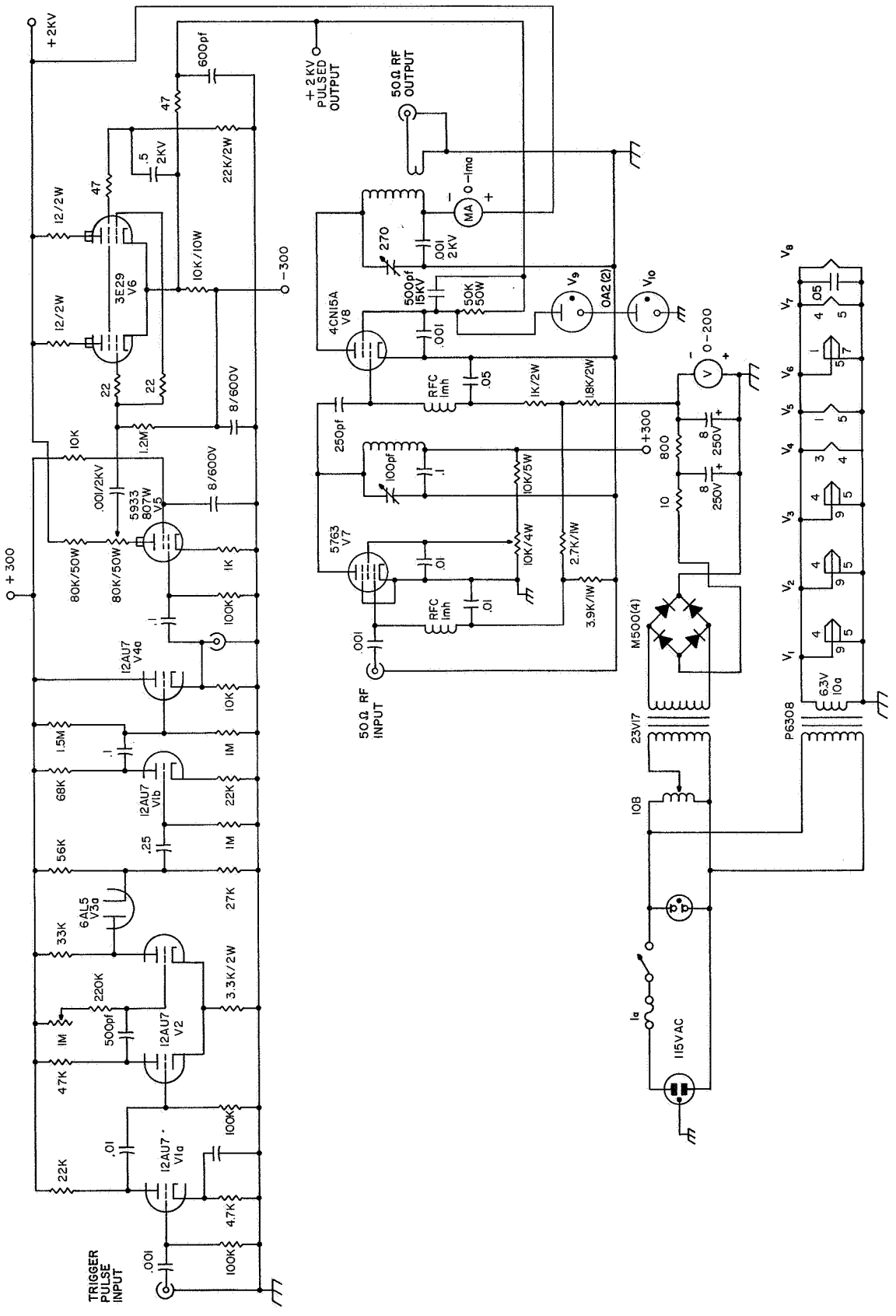

Figure 2.4 Excitor and pulse modulator (after Henry, 1966).

The plate circuit of the amplifier is a conventional push-pull balanced tuned circuit designed for a loaded Q of approximately 12. The secondary winding drives the grids of the final amplifier tubes directly. The plate circuit is tuned with a large 100 PF variable capacitor. The circuit diagram is given in Figure 2.5.

2.1.4 Final Amplifier Unit

The final amplifier stage employs two RCA 7214 ceramic tetrode tubes in a push-pull configuration to deliver 50 Kw of RF energy to the antenna. The type 7214 was chosen because of its small size, high performance at low plate voltages and relatively high power gain. The filaments of the 7214's have a rather high current requirement (17.5 amp per tube) necessitating the use of separate filament transformers for each tube. The filament voltage of each tube is completely adjustable from 0 to 5.6 V AC to permit gradual application of filament voltage.

Three blowers and a rotary fan at the top are used to cool the 7214 tubes and other components inside the final amplifier cabinet.

The screen grids of the 7214's are keyed with a 1000 volt pulse generated by a pulse modulator similar in design to that described previously in connection with the exciter stage.

The plate circuit of the final amplifier stage is a balanced push-pull tuned circuit designed to have a loaded Q of approximately 15 at the final output plate-to-plate impedance of 550 ohms. A high capacitance (1700 PF maximum), 1500 volt vacuum variable capacitor is used to tune the plate circuit.

The plate tank of the final amplifier matches the 50 ohm, unbalanced coaxial cable to the balanced 550 ohms plate-to-plate impedance of the tubes. The minimum loaded Q of the tank circuit is 10 in the operating frequency range.

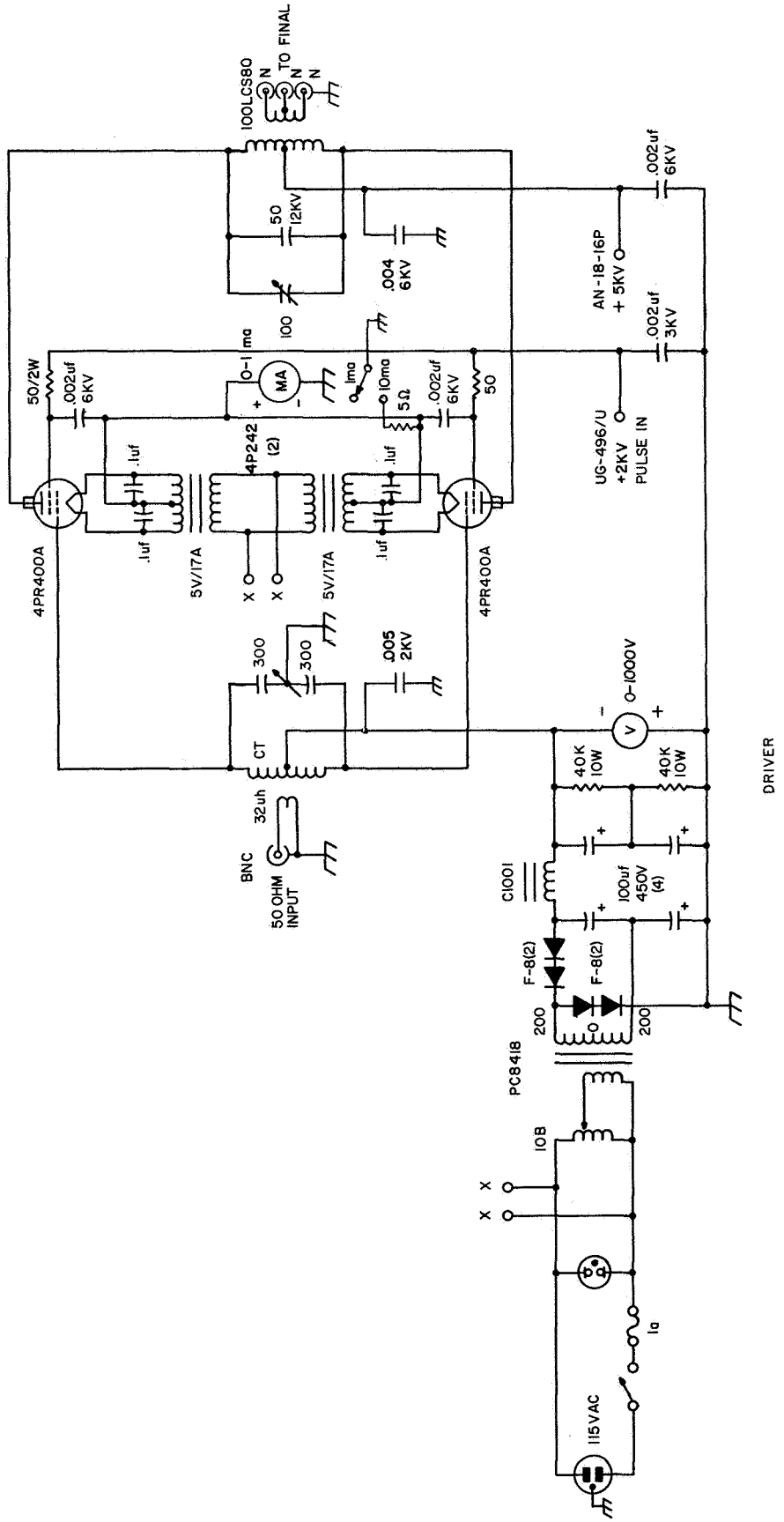

Figure 2.5 Driver amplifier (after Henry, 1966).

Additional cooling arrangement of the final amplifier was found necessary and the improved final amplifier circuit diagram is shown in Figure 2.6.

2.2 Switched Preamplifier Chain

Use of the receiver in an ionospheric drift system requires that the reference level of the receiver output be switched to three different voltages so that three concurrent signals could be displayed on an oscilloscope screen and photographed. This function is provided by means of an electronically switched preamplifier that would select one of the three spaced antennas upon command from the timing and control system.

The switched preamplifier uses three broadband RF amplifier stages. The output tuned circuit of each amplifier is designed to drive a 50 ohm coaxial cable. All components of the three amplifiers, particularly the transformers and transistors, have been matched as closely as possible to assure that the gain and phase characteristics of each channel are nearly identical. The channel switching operation is accomplished by gating the base bias circuitry of each amplifier. A positive pulse applied to the 2N697 gate transistor applies a positive pulse to the amplifier bias circuit. The amplitude of this pulse is limited to 10.0 volts by a 1N961 zener diode to assure that the amplifier gain is the same for each gate pulse. A blanking gate generator is included to provide blanking of all three amplifiers during the transmitter pulse.

The three spaced antennas are connected to the three inputs of the unit. Three gate pulses, generated by the timing and control system, gate the preamplifiers on and off in sequence. The outputs of the three switched amplifiers are mixed and connected to the input of the receiver. The sequencing of the gate pulses to the switched amplifier and those applied to the three-level switching circuit in the receiver DC amplifier is such that the "A" trace occurs

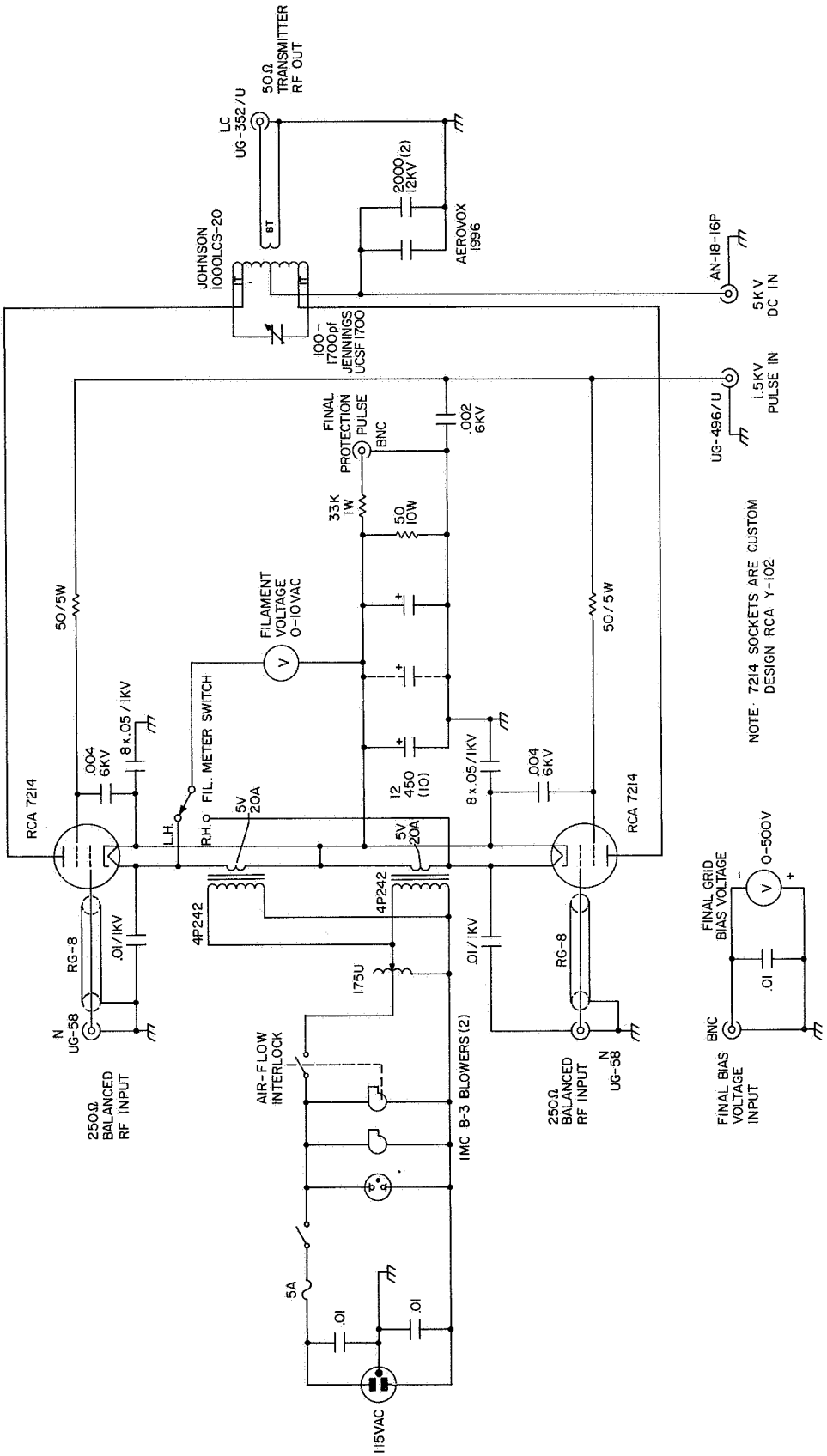

Figure 2.6 Improved final amplifier (after Henry, 1966).

first in time and is displayed at the top of the oscilloscope screen with the "B" and "C" pulses appearing in sequence thereafter. Each amplifier is capable of a maximum gain of 16 dB and a gain control dynamic range of 36 dB. Input signal for output S/N = 1; 0.32 μv. The bandwidth of each preamplifier is approximately 8.92 MHz. The schematic diagram of the electronically switched preamplifier is found in Figure 2.7.

The method of shifting the oscilloscope vertical position for each pulse has been modified. The original system used DC level shifting in the DC amplifiers of the receiver to achieve the required position change. A new level shifting circuit has been designed that simply switches vertical position controls in the oscilloscope, allowing greater versatility in the system. Gate pulses are used to trigger relays which select one of the three position controls of the oscilloscope.

2.3 Pulse Receiver

1.	RF center frequencies	Tunable from 2.00 to 3.50 MHz or fixed frequencies at 2.66 MHz.
2.	Noise figure	3 dB maximum.
3.	Bandwidth	50 kHz at -3 dB points on bandpass response curve.
4.	Ripple within passband	3 dB overall maximum.
5.	Manual gain control	Sufficient to adjust for an input variation over the range of 1.0 microvolt to 1.0 millivolt.
6.	Recovery time	200 microseconds for receiver to drop into noise after 0.1 volts rms at the signal frequency applied at the input is removed.

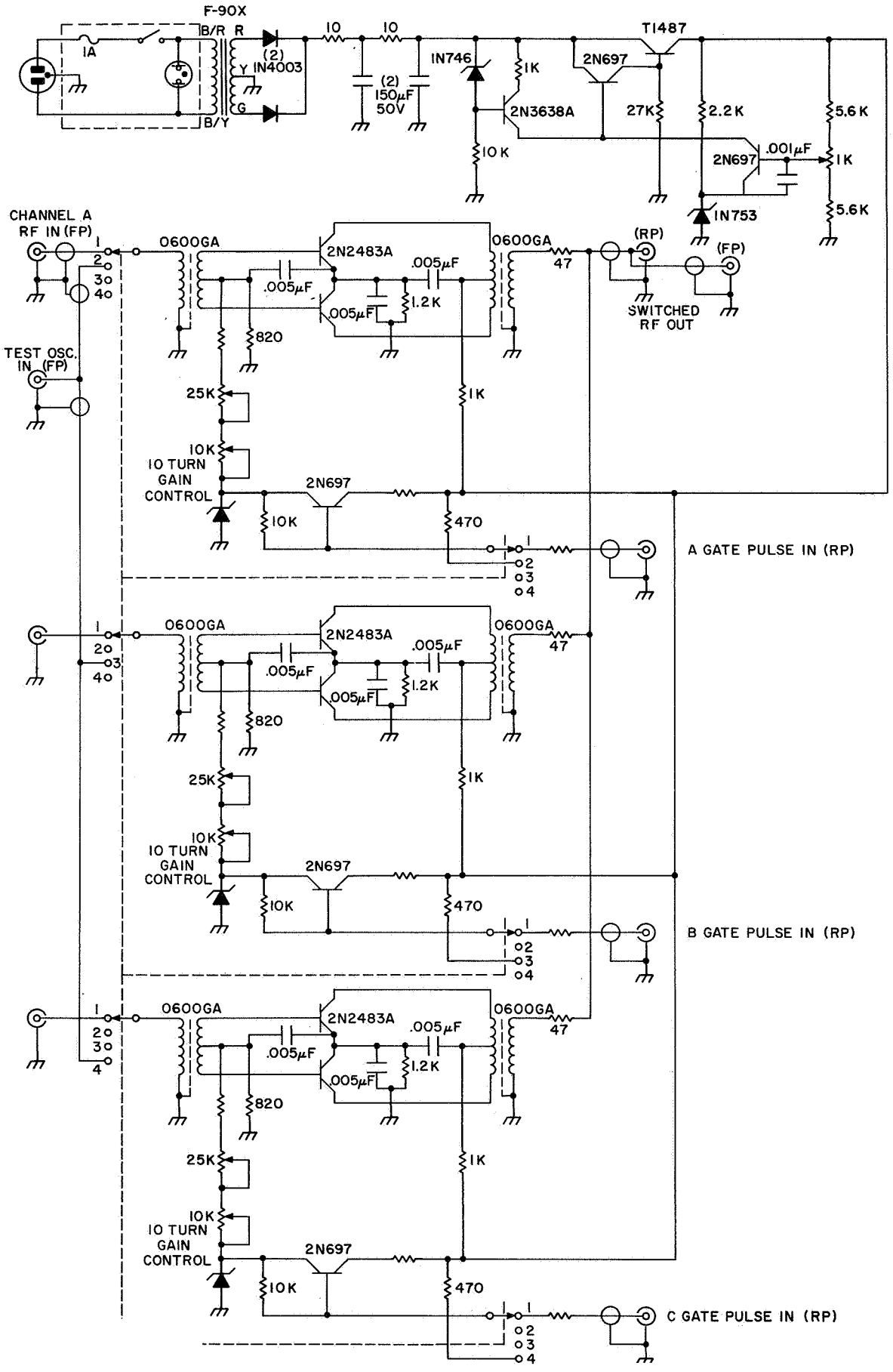

Figure 2.7 Electronically switched preamplifiers.

7.	Gain variation	3 dB maximum over the temperature range of 15°C to 35°C.
8.	Power supply	All voltages to the receiver are regulated to within 0.1% for AC line voltage variations of 10% and over the temperatures of 15°C to 35°C.
9.	RF input impedance	50 ohms unbalanced.
10.	Output impedance	10,000 ohms maximum, unbalanced.
11.	Gain per stage	
	RF amplifier	20 dB
	Mixer	10 dB
	IF amplifier	20 dB each, 80 dB total for 4 stages
	Detector	-10 dB
	DC amplifier	20 dB
	Maximum receiver gain	120 dB

This gives for an input signal of 1.0 microvolt at 50 ohms an output of 10 volts at 10,000 ohms.

To avoid problems of strong adjacent-channel signal cross modulation, the gain before the bandwidth-determining IF amplifier chain was purposely kept low.

Discussion of the design of the receiver is divided into the following sections, in which the various units are described individually:

RF amplifier, mixer and local oscillator unit.

IF amplifier, detector and DC amplifier unit.

Power supply unit. Receiver performance characteristics.

2.3.1 RF Amplifier, Mixer and Local Oscillator Unit

The RF amplifier, mixer and local oscillator circuits as well as the blanking pulse generator stages are all incorporated in one plug-in unit of

the receiver. All circuitry of the unit is constructed on 1/16-inch copper-clad circuit boards, and shield plates are used between each stage to minimize interaction and prevent instability.

The RF amplifier stage is designed to operate as a neutralized tuned amplifier, using tuned transformers for impedance matching and neutralization feedback. The transformers have been designed and constructed using Cambridge Thermionic Corporation Type 1181 shielded coil form and core assemblies and No. 5-44 litz wire. Use of the CTC form, litz wire, and bifilar winding achieved coefficients of coupling of approximately 0.9, making double tuning of the transformers uncecessary. Neutralization of the RF amplifier is accomplished by feedback to the transistor base of a position of a signal which is 180 degrees out of phase with the collector signal. The amount of feedback is controlled by the size of the neutralizing capacitor and the turns ratio between the collector and feedback windings. To assure close coupling between these two windings, the neutralization winding is actually wound as a portion of the collector winding, with the collector DC supply connected to a tap on this winding. To assure close coupling between the collector and output windings, the two are bifilar wound, with the secondary winding starting at the collector DC supply tap.

2N2483 transistors are used for the RF amplifier and mixer units. These transistors are capable of giving a low noise figure required in the 2 to 10 MHz frequency range. In the interest of economy and standardization, 2N24835 are also used in the IF amplifier stage of the receiver.

For optimum gain and noise performance, the 2N2483 transistor base is matched to an input impedance of 7,500 ohms and the transistor itself is operated at I_e=1.0 ma (DC bias). The input transformer matches the base to a 50 ohm

coaxial cable, the input to the receiver. The gain of the RF amplifier stage is controlled over a 25 dB dynamic range by varying the DC base bias of the 2N2483. The mixer stage also employs a 2N2483 transistor matched for a base impedance of 7,500 ohms and DC biased for I_e=1.0 ma. The RF input signal is injected to the base of the mixer transistor by the output transformer of the RF amplifier stage. The IF output is transferred from the collector of the mixer by means of a tuned transformer that matches the IF signal to a 100 ohm coaxial cable for transmission to the IF amplifier module. The local oscillator signal is injected in the emitter circuit of the mixer by means of an isolating emitter follower that shares a common emitter resistance with the mixer transistor. The emitter follower stage again uses a 2N2483 transistor at a DC bias of I_e=1.0 ma. Use of the emitter follower stage minimizes the possibility of the local oscillator being pulled in frequency by a very strong signal at the RF input frequency of the receiver.

The local oscillator stage uses a 2N706 transistor in a colpitts type of circuit. The crystal is operated in its series resonant mode in series with the feedback path. The amount of feedback is controlled with a capacitive voltage divider system across the collector tuned circuit. The oscillator DC collector voltage is doubly regulated, first by the main +15 volt regulator and then by a 10 volt zener diode, to assure stable operation under all conditions. The local oscillator input signal is also coupled to the emitter-follower stage by means of a capacitive voltage divider. Approximately 1% of the total oscillator collector signal is required to give proper injection to the mixer, affording a still greater degree of isolation for the oscillator.

In order to protect the RF amplifier transistor and also to prevent the receiver from saturation it is desirable to provide some means of disabling the

receiver during the transmitter operation time. The receiver blanking circuit provides this by shorting the RF input to the receiver during the transmission pulse.

Construction of the RF amplifier, mixer and local oscillator stages follows conventional construction practices for high frequency designs; all signal leads are kept as short as possible, extensive shielding is used to separate each RF circuit from the others, all DC and control lines are bypassed with as short leads as possible. The schematic diagrams of the RF stages are given in Figure 2.8.

2.3.2 IF Amplifier, Detector and DC Amplifier Unit

The IF amplifier portion of the receiver consists of four neutralized tuned amplifier stages again using single-tuned transformers to achieve neutralization and impedance matching. The input transformer matches the 100 ohm coaxial cable from the RF amplifier module to the base of the first transistor amplifier. Three interstage coupling transformers are used, one between each amplifier stage. The output transformer matches the collector of the output transistor amplifier to the detector system.

A frequency of 5.0 MHz is chosen for the IF frequency because of the wide bandwidth required of the receiver. If a frequency of approximately 1.0 MHz were used, the loaded Q of each tuned circuit would have to be much too low (15 or less) to allow for any skirt selectivity. The overall IF bandwidth is 50 kHz. Using five single-tuned, isolated transformers, the bandwidth of each transformer must be 50/.386 = 130 kHz. At a center frequency of 5.0 MHz, a loaded Q of 38 (Landee et al., 1957) will result in this bandwidth. A Q of 38 is readily obtainable from the CTC coils and allows for fairly steep skirt selectivity.

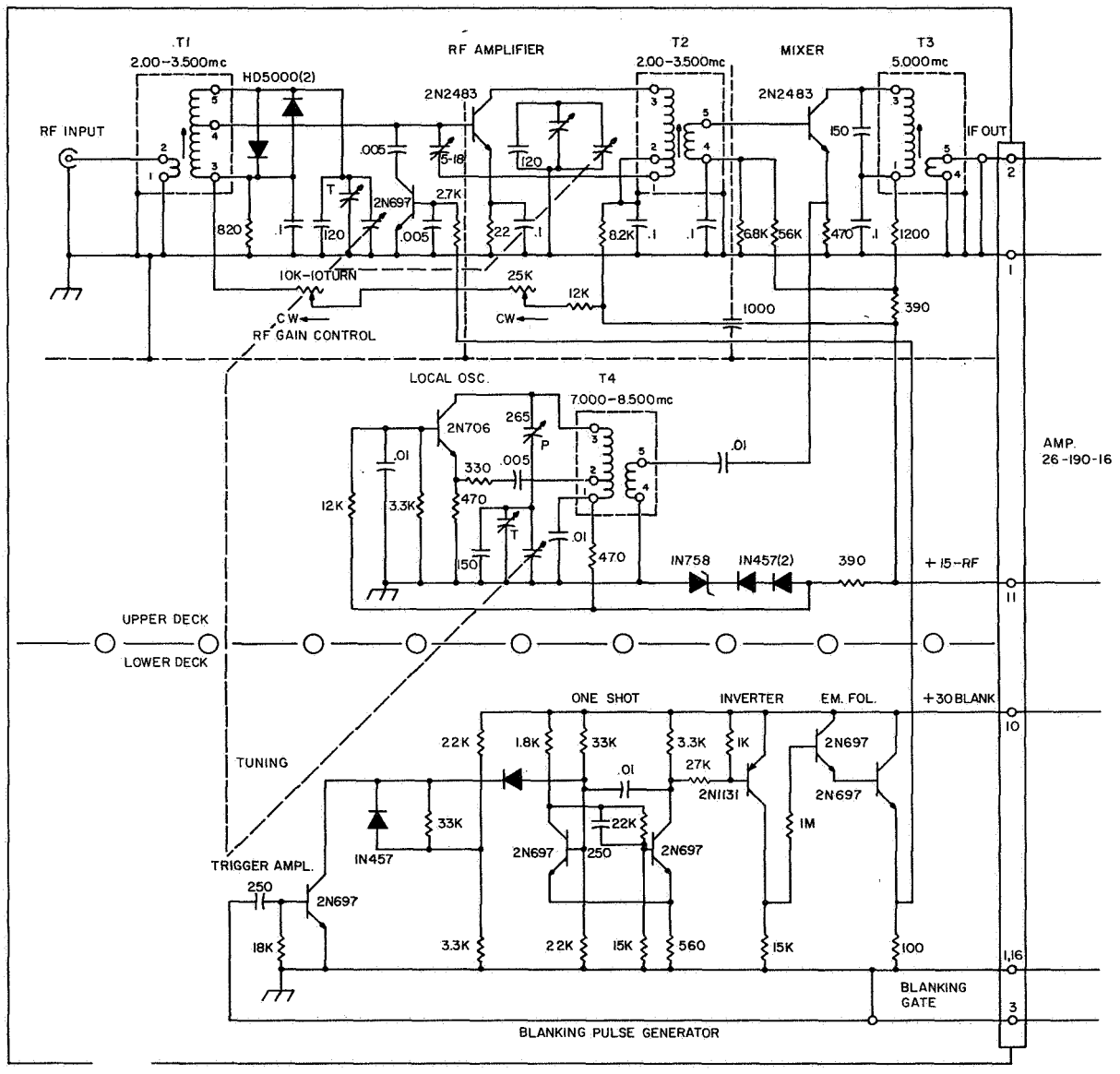

Figure 2.8 RF stages of the receiver (after Henry, 1966).

As in the RF amplifier and mixer stages, 2N2483 transistors were used as amplifier transistors. As before, the 2N2483 is DC biased for I_e=1.0 ma. Gain control of the IF amplifier chain is accomplished by varying the base bias of the first and third amplifiers. The overall dynamic range of the IF gain control is approximately 45 dB.

The detector stage consists of four matched 1N63A germanium diodes connected in a full-wave bridge circuit. This circuit was chosen over the more conventional half-wave detector system because of the inherent reduction in pulse distortion with the full-wave system. The detected signal is of an average level of 0.5 volts, sufficiently high to be easily amplified by the DC amplifier stage.

A standard differential amplifier is used in the DC amplifier stage. An MD1120 dual matched transistor device is used in the differential amplifier. The MD1120 consists of two closely matched (all parameters within 1%) NPN silicon transistors in one TO-5 case. Since both semiconductors are in one package, differential temperature drifts are nearly impossible. A 2N697 is used as a 1.0 ma constant current source in the emitter circuit of the differential amplifier to assure high common-mode rejection. A 2N1131 transistor is used as an inverter and DC level-shifting stage following the differential amplifier. The circuit diagrams of the IF stages are shown in Figure 2.9.

Since the receiver is intended for use in reception of pulsed RF signals, its response to a pulsed signal is definitely of interest. Figure 2.10 shows a typical output obtained from the receiver with a square RF pulse input (the RF input pulse is the upper trace and the receiver output is the lower trace). Since the receiver bandpass of 50 kHz is only sufficient for the 5th order sidebands of a 50 μsec square pulse, the output pulse is rounded and has a Gaussian

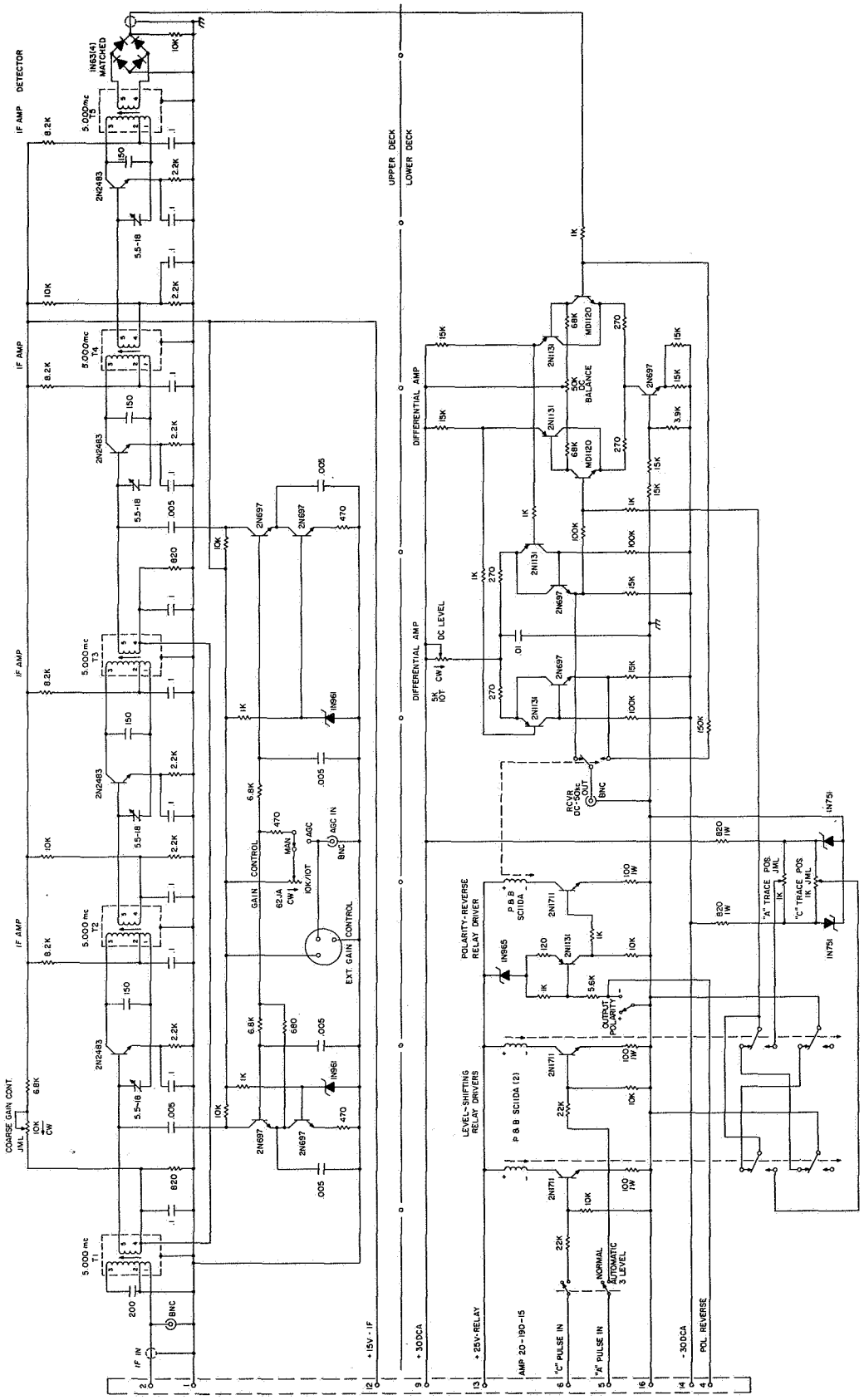

Figure 2.9 IF detector and DC amplifier (after Henry, 1966).

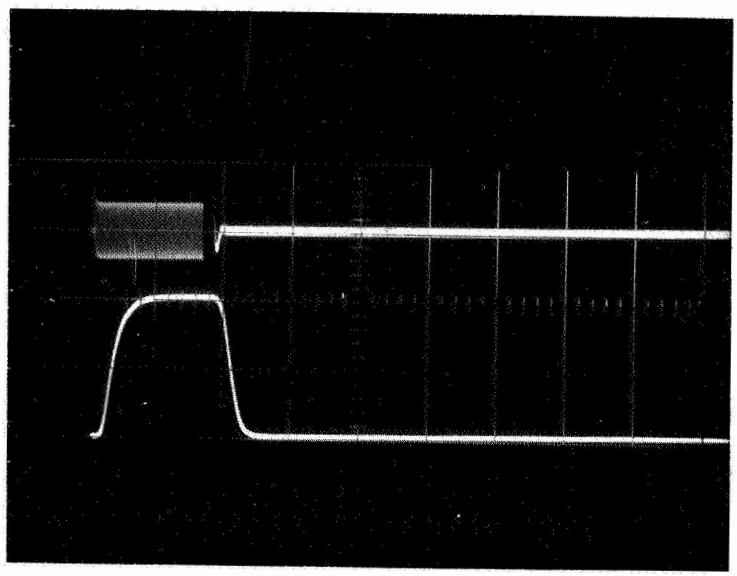

Figure 2.10 Receiver pulse response (after Henry, 1966).

shape. The time delay between the input pulse and the output pulse represents the actual time delay of the receiver. As long as the phase shift of the receiver is a linear curve within the receiver bandpass and the time delay does not change with receiver gain, this delay is easily cancelled out in the data reduction process or, in the case of filmed recording, the oscilloscope trace is simply delayed by an amount equal to the time delay of the receiver. The most recent timing and control systems designed include a provision for a delayed trigger to provide compensation for both receiver and transmitter-originated delays.

The measured receiver sensitivity is 0.4 μvolt of signal for an observed S/N ratio of 1.00. Taking into consideration bandwidth of the receiver, the noise figure was calculated to be approximately 2.0 dB, depending upon the accuracy with which a signal-to-noise ratio of 1.00 can be measured. In practice, this sensitivity has proven to be more than that required, because of the high level of man-made and atmospheric noise at the frequencies of interest.

The gain of the receiver has been measured as constant within 1.5 dB over an eight-hour period of operation in a sounding system. This gain change has been traced to h_{fe} variations of the RF amplifier transistor with temperature and, to a smaller degree, to drift of the power supply regulator voltage.

The crystal-controlled local oscillator stability was measured to be within 500 Hz of center frequency 15 minutes after turning the receiver on and within 100 Hz throughout the remainder of an eight-hour operation schedule. The tunable oscillators used in the RF-3 and RF-4 modules have a short-term stability of ±250 Hz.

2.4 Antennas

The receiving aerials for the drift experiment consists of ten turns of vertical coaxial loops placed at the corners of an equilateral triangle in the directions as shown in Figure 2.11. The plane of the loops are kept parallel. The loops are constructed of RG.8/U coaxial cable and were impedance matched at the end of the 333 ft feedline at the receiver terminals. The area of the loops are approximately one square meter.

The transmitting antenna is a large array consisting of 50 collinear dipole elements, arranged in two sets of 25 each with one set physically perpendicular to the other. All 25 elements in one set is fed in phase with each other and the two sets are phased in quadrature to achieve either mode of circular polarization. The lines of half-wavelength dipole elements are separated by one-half wavelength at 2660 kHz. The transmitter power is fed to each of the dipoles by a phased array feed system. A total of 80 class-2 70 ft treated southern yellow pine utility poles support the two 50 element arrays. The diagram of the array is shown in Figure 2.12. A calculation of directive gain of the array based upon effective antenna area predicts that a gain of approximately 28 dB over an isotropic-radiator was to be achieved with each antenna array.

2.5 Camera and Time Marker System

A continuous moving 35 mm film magazine photographs the fading records. The film speed has been kept low. Approximate speed is about 1.4 inch per minute. The camera motor is actuated by the timing circuit of the system and starts and stops accordingly. The drift data is taken daily on every hour for 15-minute intervals, starting from 0845 hours in the morning to 1945 hours in the afternoon.

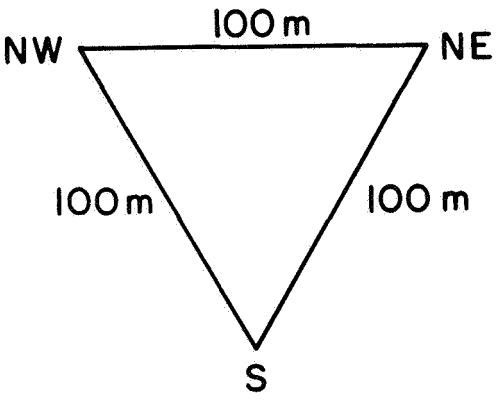

Figure 2.11 Receiving antenna arrangement

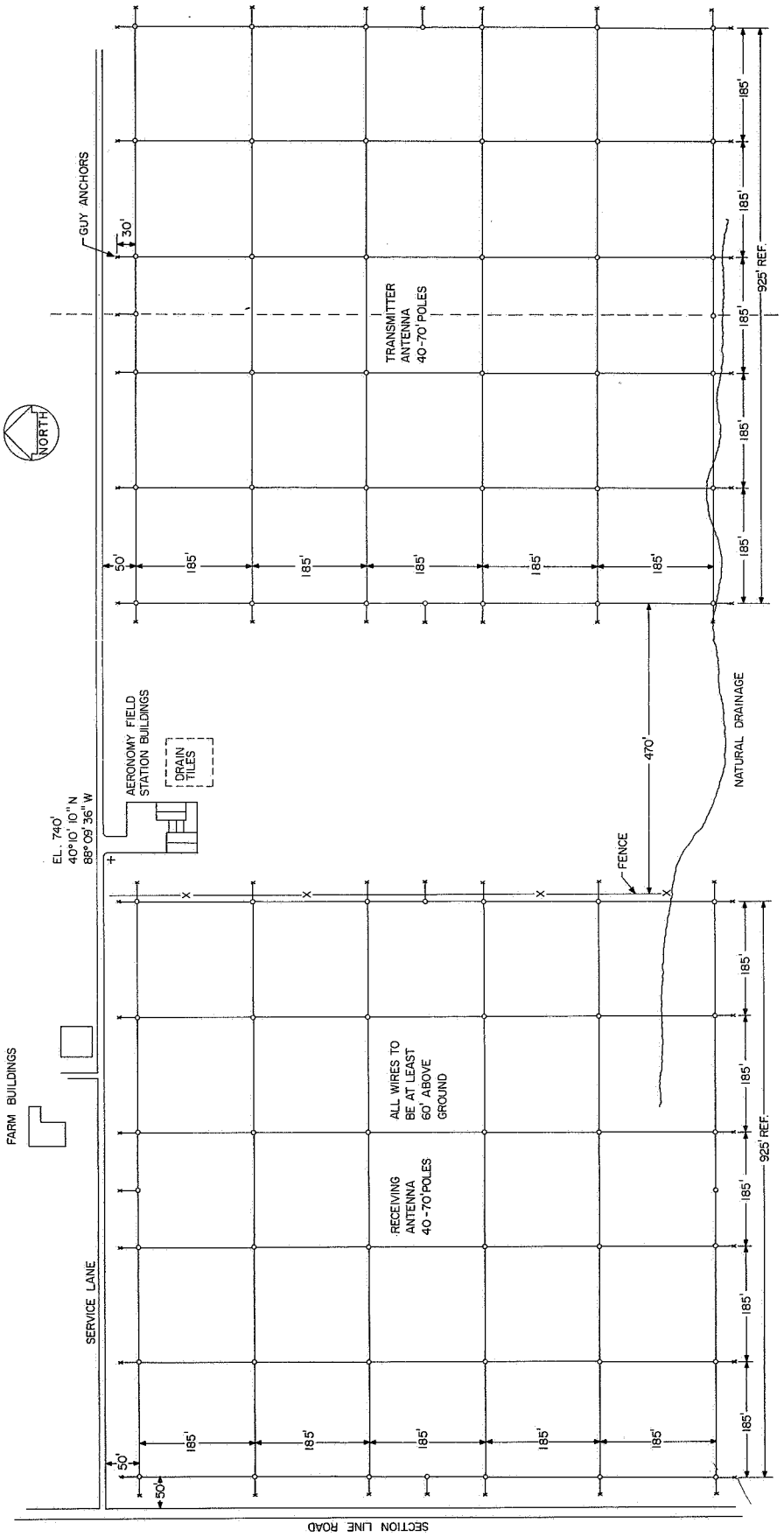

Figure 2.12 Transmitting antenna arrangement.

The time marker generator provides time reference marks on the data record at 5-second intervals. The unit uses a synchronous timing motor and simple logic circuit to blank the oscilloscope unit at the appropriate time for a period of 100 milliseconds.

3. METHODS OF ANALYSIS

3.1 Definitions and Basic Equations

It is necessary to define some basic quantities for measuring the drift velocity and the structure of the irregularities. These basic definitions are derived from the fading records of the three receivers. They will be explained below.

3.1.1 Correlation Functions

The most important statistical quantity used in this method of analysis of time series is the correlation function, defined for one direction, as

$$\rho(\tau,\xi) = \frac{\overline{[R(x,t) - \bar{R}][R(\chi+\xi,\ t+\tau) - \bar{R}]}}{\overline{[R(x,t) - \bar{R}^2]}} \tag{3.1}$$

where $R(x,t)$ is the signal amplitude at a receiver located at position x at time t. A bar drawn over any quantity denotes the average of that quantity over a time which is long, compared with the time scale of the variation in the quantity.

Two special cases of Equation (3.1) are the auto- and cross-correlation functions, defined respectively as

$$\rho_a(\tau) = \frac{\overline{[R(\chi,t) - \bar{R}][R(\chi,t+\ ) - \bar{R}]}}{\overline{[R(x,t) - \bar{R}]^2}} \tag{3.2}$$

and

$$\rho_c(\varepsilon_o,\tau) = \frac{\overline{[R(x,t) - R][R(x+\varepsilon_o,t+\tau) - \bar{R}]}}{\overline{[R(x,t) - \bar{R}^2]}}$$

where ε_o is the separation between the two receivers. Typical forms for these functions are shown in Figure 3.1.

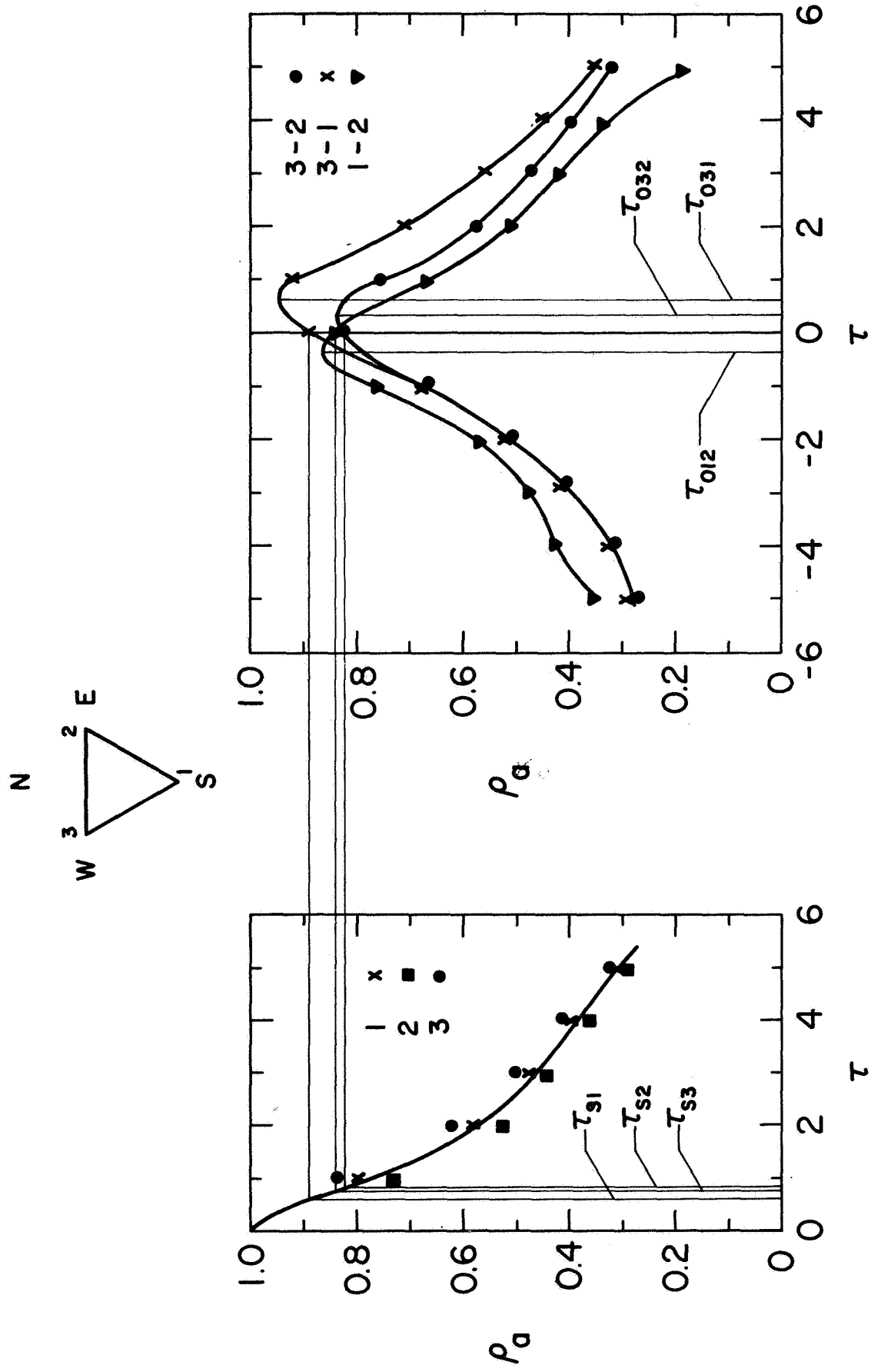

Figure 3.1 Typical auto-and cross-correlograms.

The functional form of an autocorrelation function may be described mathematically as:

$$\rho_a(o) = 1$$

$$\rho_a(\tau_1) > \rho_a(\tau_2) \qquad \tau_2 > \tau_1$$

$$\rho_a(\tau) = \rho_a(-\tau)$$

τ denotes the time interval.

The cross-correlation function $\rho_c(\varepsilon_o,\tau)$ behaves similarly except that its maximum value is not necessarily located at τ=0, and since the cross-correlation function uses two time series, which are not necessarily identical, the maximum value of correlation is not usually unity, the maximum value at τ_o of $\rho_c(\tau_o)$ is $\leq$ 1 depending on the similarity between the two series.

The use of correlation functions in this work requires that the time series be statistically stationary. That is, important statistical parameters, such as mean amplitude and standard deviation, do not vary over the length of time for which the analysis is being carried out.

3.2 Velocities

Briggs, et al. (1950) defined four velocities in order to describe the motion of the diffraction pattern over the ground. The two fundamental velocities are the drift velocity V_D and the short period random velocity V_R. The other two velocities are derived velocities and are defined as follows:

3.2.1 V', Fictitious Drift Velocity

Fading records from two receivers separated by a distance ε_o, are compared for maximum cross-correlation, which is found to occur at a time lag τ_o. Then V_1', that is V' in the direction of the two receivers, is given by $V_1' = \frac{\varepsilon_o}{\tau_{o_1}}$. Similarly for two other receivers separated by η_o in a different direction, V_2' is defined as $V_2' = \frac{\eta_o}{\tau_{o_1}}$.

3.2.2 V_D, Steady Drift Velocity

The velocity with which the pattern drifts over the receivers. It is assumed that this does not change within the length of the time of the record analyzed.

3.2.3 V_R Short Period Random Velocity

The minimum fading speed is observed when a receiver is moved with the pattern with velocity V_D. This minimum fading rate is explained in terms of random motions of the pattern on the ground. The short period random velocity V_R is the velocity with which a frozen pattern must drift so that this minimum fading rate is observed.

3.2.4 V_R' Fading Velocity

As mentioned above, the fading of the reflected radio signal arises from two sources, steady drift and random motions of ionospheric irregularities. If the pattern is imagined to be "frozen" at any instant of time so that no random changes occur, the question is asked, "at which velocity should this 'frozen' pattern move so that the signal fades at the rate found for the original changing pattern?" This velocity is denoted by V_R'. It is obvious that if there are no random motions, fading velocity should be equal to the drift velocity. This velocity is derived from the fading records by the method shown below. Fading

velocity $V_{R1}' = \frac{\varepsilon_o}{\tau_{s1}}$ in the direction of the two receivers separated by ε_o, where τ_{s1} is obtained from the relation

$$\rho_c(\varepsilon_o, o) = \rho_a(o, \tau_{s1})$$

where ρ_c and ρ_a are previously explained and the time lags τ_o and τ_s are shown in Figure 3.1.

Briggs, et al. (1950) also showed that for an isotropic ground pattern

$$V_R'^2 = V_D^2 + V_R^2$$

and (3.3)

$$V_D V' = V_R'^2$$

It is therefore clear that by measuring τ_o and τ_s from the correlograms of the fading records we can determine the drift and random velocities. The above analysis is uncorrected for anisotropy of the ground pattern; this aspect has been taken care of by correction terms which involves the axial ratio and tilt angle of the correlation ellipse and will be explained in the later part of this chapter. The main difference between the methods of Briggs, et al. (1950) and of Lee (1962) lies in the determination of τ_o and τ_s from the fading records. As explained in the introduction, we are following the Lee method for measuring the above parameters. Hence it is necessary to explain it in detail.

3.3 Methods of Measuring τ_o and τ_s Assuming Gaussian Distribution

The meaning of τ_o and τ_s will be clear from the Figure 3.1 which is a plot (in same scale) of auto- and cross-correlation functions of the fading records from the three receivers. The auto-correlogram is plotted by taking

the mean values of the three records. It is assumed that both auto- and cross-correlograms obey Gaussian distribution, i.e. they are respectively

$$\rho_a(\tau) = \exp\left[-\frac{\tau^2}{2b^2}\right] \tag{3.4}$$

where b is a constant and $\rho_a(o) = 1$ and

$$\rho_c(\varepsilon,\tau) = \rho_o \exp\left[-\frac{1}{2\beta^2}(\tau-\tau_o)^2\right] \tag{3.5}$$

where B is a constant and ρ_o is the maximum value of ρ_c.

The following steps are taken for the measurement of τ_o and τ_s.

(1) RO is calculated.

where $$RO = \frac{(\rho_a)_1 + (\rho_a)_2 + (\rho_a)_3}{3} \tag{3.6}$$

where $(\rho_a)_1$ = autocorrelation function for receiver I at time $\tau = 1$

$(\rho_a)_2$ = autocorrelation function for receiver II at time $\tau = 1$

$(\rho_a)_3$ = autocorrelation function for receiver III at time $\tau = 1$.

According to our definition

$$RO = \exp\left[-\frac{1}{2b^2}\right] .$$

Hence $-\frac{1}{2b^2} = \log_e RO$.

Substituting this in (3.4)

$$\rho_a = \exp(\tau^2 \log_e RO) \tag{3.7}$$

$$\tau^2 = \frac{\log_e \rho_a}{\log_e RO} .$$

Let the values of cross correlation functions between the records I, II and III at $\tau=0$ be ρ_{031}, ρ_{032}, ρ_{012}.

(2) the values of τ_s are

$$\tau_{s1}^2 = \frac{\log_e \rho_{031}}{\log_e RO}, \quad \tau_{s2}^2 = \frac{\log_e \rho_{032}}{\log_e RO}, \quad \tau_{s3}^2 = \frac{\log_e \rho_{12}}{\log_e RO}.$$

(3) To determine τ_o let us examine the cross-correlation function between the records I and III shown in Figure 3.1. This function $\rho_c = \rho_o e^{-(\tau-\tau_{o1})^2/2B^2}$. Let us take three values of the above function: ρ_{031} at $\tau=0$; ρ_{131} at $\tau=1$; and ρ_{113} at $\tau=-1$, as shown in Figure 3.1.

We then get three equations:

$$\rho_{031} = \rho_o e^{-\tau_{o1}^2/2B^2}$$

$$\rho_{131} = \rho_o e^{-(1-\tau_{o1})^2/2B^2}$$

$$\rho_{113} = \rho_o e^{-(1+\tau_{o1})^2/2B^2}$$

On eliminating ρ_o and solving for τ_{o1},

$$\tau_{o1} = \frac{\log_e \rho_{131} - \log_e \rho_{113}}{4\log_e \rho_{031} - 2\log_e \rho_{131} - 2\log_e \rho_{113}} \quad . \tag{3.8}$$

Similarly τ_{02} and τ_{03} are obtained. Once the values of τ_o and τ_s are determined by the above method the fading velocity V_R' and fictitious drift velocity V' can be determined in three directions and the values of drift velocity and random velocity can be obtained from Equation (3.3) in the three directions of the receivers. It is assumed that the mean random velocity is isotropic.

Up to this point we have determined the velocity of the blob with the assumption of statistically isotropic amplitude variation on the ground. In practice there is considerable deviation from this condition, and an anisotropic amplitude pattern may be approximated statistically by an ellipse with axial ratio s and tilt angle ψ of the major axis measured from some reference direction.

The spatial structure in a given direction is defined as the separation between two points such that the correlation of amplitude between the points is $1/\sqrt{e}$, or 0.61. For an anisotropic pattern this structure size is a function of the angle which the line joining the two points makes with an arbitrary reference direction. The values of the velocities obtained as above will be modified due to this anisotropy and some correction factor is necessary. Let us first determine the correlation ellipse and then the corrections to the velocity will be applied to the results obtained above.

3.4 Spatial Correlation Ellipse and Structure Size

The determination of the structure size, as defined above, requires an assumption concerning the form of the spatial autocorrelation function. In fact, this experiment measures only one point on the spatial autocorrelction function for any given direction. This point is part of the temporal cross-correlation function of the amplitudes at the two receivers, namely $\rho_c(0,\varepsilon_o)$. That is, the cross-correlation coefficient for zero time lag is a point on the spatial autocorrelation function. Knowing one point on the spatial correlation function is not sufficient to determine the structure size d_{ij} in the direction of the time joining receivers i and j. The quantity d_{ij} is expressed in terms of the spatial correlation function as $\rho_s(d_{ij}) = 0.61$. A knowledge of the shape of ρ_s is necessary for the determination of d_{ij}.

Two propositions were considered for the shape of the spatial auto-correlation function. The first, advanced by Bowhill (1956), is here called the "Gaussian approximation". The second is by Brennan (1960), and is here called the "similarity hypothesis". These terms have the following significance.

(1) The "Gaussian approximation" is to take a Gaussian form for the spatial correlation function, represented by

$$\rho_s(\varepsilon) = \exp(-\varepsilon^2/2d_{ij}^2) \quad .$$

Bowhill determined this form from experiments with two receivers at different separations.

(2) The "similarity hypothesis" results for measurements made again at several receivers arranged in a straight line with varying separation. The results as stated by Brennan (1960), are that the shape of the spatial auto-correlation function is the same as the temporal auto-correlation function. It is easy to see that if $V_r=0$, that is, there is only a drift motion, then the temporal and spatial auto-correlation function are identical, except for a proportionality factor. His important result is that even when $V_r\neq 0$, the spatial function can be derived simply from the temporal function by a constant proportionality factor.

The importance of this "similarity hypothesis" is that from the temporal function and one point on the spatial function, the entire spatial function can be estimated. Once the spatial function is known, the structure size can be easily calculated. If the temporal function should turn out to be Gaussian in shape, then, by the "similarity hypothesis", the spatial function will also be Gaussian.

Taking into consideration of the above assumptions the structure size is determined from $d_{ij} = (\varepsilon_o/\tau_x)\tau_s$, where τ_x is defined as $\rho_a(\tau_x) = 0.61$. τ_x can be calculated very easily from the auto-correlation functions obtained previously and we have

$$\tau_x = \sqrt{\frac{\ln 0.61}{\ln RO}} = 1/\sqrt{2 \ln RO}$$

and τ_s was previously obtained. Substituting the values of τ_s obtained along the three receiver directions, the structure size along those directions are obtained. The spatial correlation ellipse defined by $\rho_s = 0.61$ can be given by the general equation of an ellipse

$$Ax^2 + Bxy + Cy^2 = 1 \tag{3.9}$$

where A, B, C are constants. This is the equation of an ellipse with center at the origin and with axial ratio

$$s = \frac{(A+C) + \sqrt{4B^2+(A-C)^2}}{(A+C) + \sqrt{4B^2+(A-C)^2}} \quad . \tag{3.10}$$

The tilt angle of the major axis measured from the x axis in the counter-clockwise direction

$$\tan 2\psi = \frac{2B}{A-C} \tag{3.11}$$

The next problem is to express these parameters in terms of the measured correlation coefficients. From the computed structure sizes, d_{32}, d_{31} and d_{12} in the W-E, W-S and S-E directions respectively the two parameters of the ellipse are to be determined. The receiver triangle is considered to be

equilateral. The positive x axis is taken along W-E line in the direction from W to E as shown in Figure 3.2. Substituting the coordinates of these three points into Equation (3.9) results for the three unknown coefficients A, B and C, the equations

$$A = \frac{1}{d_{32}^2}$$

$$C = \frac{1}{3}\left[2\left(\frac{1}{d_{31}^2} + \frac{1}{d_{12}^2}\right) - \frac{1}{d_{32}^2}\right] \tag{3.12}$$

$$2B = \frac{2}{\sqrt{3}}\left[\frac{1}{d_{31}^2} - \frac{1}{d_{12}^2}\right]$$

Substituting these values of A, C and B in Equation (3.11) gives

$$\tan 2\psi = \frac{\sqrt{3}\left[\left(\frac{d_{12}}{d_{31}}\right)^2 - 1\right]}{2\left(\frac{d_{12}}{d_{32}}\right)^2 - \left(\frac{d_{12}}{d_{31}}\right)^2 - 1} \quad . \tag{3.13}$$

Now let $r_{13} = \left(\frac{d_{12}}{d_{32}}\right)^2$, $r_{12} = \left(\frac{d_{12}}{d_{31}}\right)^2$ (3.14)

and substituting these into Equation (3.12) gives

$$\tan 2\psi = \frac{\sqrt{3}\,(r_{12}-1)}{2r_{13} - r_{12} - 1} \tag{3.15}$$

Substituting Equations (3.12) and (3.14) into Equation (3.10) gives for the axial ratio

$$s = \frac{1/2(r_{13}+r_{12}+1) + [r_{12}^2+r_{13}^2-r_{12}r_{13}-r_{12}-r_{13}+1]^{1/2}}{1/2(r_{13}+r_{12}+1) - [r_{12}^2+r_{13}^2-r_{12}r_{13}-r_{12}-r_{13}+1]^{1/2}} \quad . \tag{3.16}$$

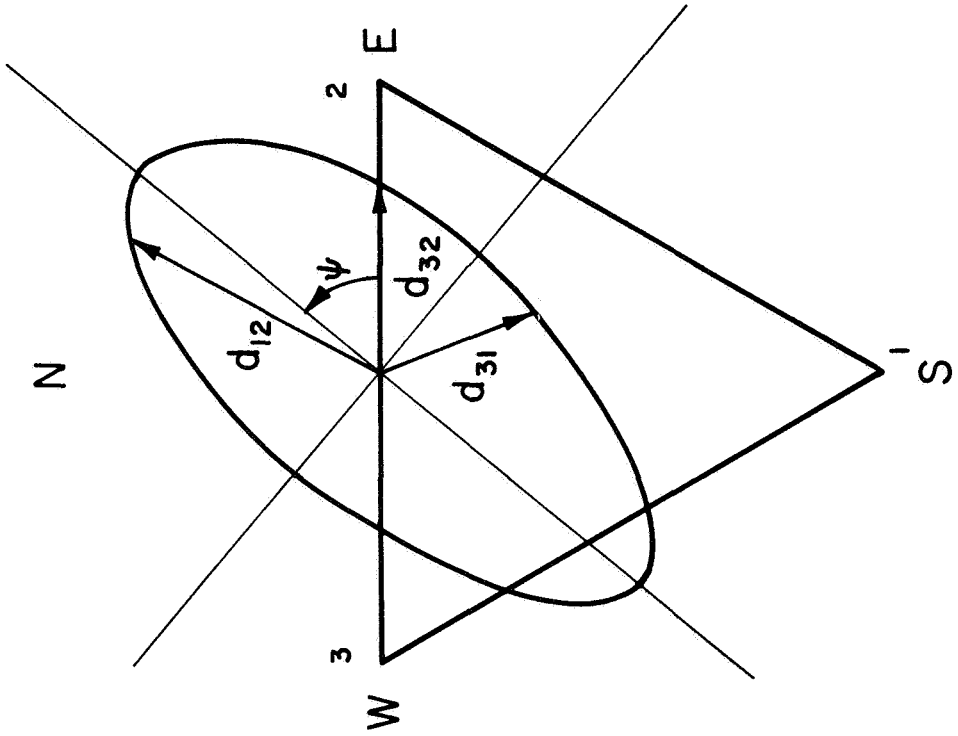

Figure 3.2 Spatial correlation ellipse in the receiver triangle.

Figure 3.2 shows the spatial correlation ellipse drawn in the coordinate system of the three receivers.

3.5 Anisotropy Correction

The method of Briggs, et al. (1950) using results from three receivers, determines values for the apparent magnitude of the drift velocity, V_{Da}, its apparent direction, ϕ_a and the apparent magnitude, V_{Ra}, of the random velocity of the pattern. For an isotropic amplitude pattern on the ground (for which the correlation function contours are circular), these apparent values are equal to the true values V_D, ϕ and V_R. Phillips and Spencer (1955) considered the effect, on the magnitude of the drift velocity, of anisotropy of the pattern; contours of spatial auto-correlation function being elliptical, with axial ratio s, and major axis direction angle ψ. They found the relationships between the apparent and true values of V_D and ϕ to be

$$\tan(\phi-\phi_a) = \frac{(s^2-1)\tan(\phi_a-\psi)}{1 + s^2\tan^2(\phi_a-\psi)} \tag{3.17}$$

$$V_D = V_{Da}\cos(\phi-\phi_a) \cdot \frac{1 + (s^2-1)\cos^2(\phi_a-\psi)}{1 + (s^2-1)\cos^2(\phi-\psi)} \tag{3.18}$$

They did not, apparently, find a similar relation for the random velocity; assuming that this random velocity may have any direction relative to the drift velocity with equal probability, it can be shown that

$$V_R = V_{Ra}\cos(\phi-\psi) \sqrt{\left(2\frac{1 + s^2\tan(\phi-\psi)}{1+s^2}\right)}. \tag{3.19}$$

While this correction is small for nearly isotropic patterns, an axial ratio of 1.4 may produce a 2:1 variation of V_R, depending on the drift direction relative to the major axis of the correlation ellipse. This correction would become very important where highly anisotropic patterns are encountered.

3.6 Sampling Theory and Determination of Sampling Interval

The aspect of sampling theory to be treated here deals with errors which arise in the calculation of correlation coefficients due to the finite length of records analyzed. It is hypothesized that each 15 minute long record analyzed is a sample taken from an infinitely long record with mean amplitude μ, variance σ^2 and auto-correlation function $\rho(\tau)$. From the finite sample a mean amplitude m, variance s and correlation function $r(\tau)$ are computed.

The subject of this section concerns the reliability of $r(\tau)$ as an estimate of $\rho(\tau)$, and the errors arising from the use of $r(\tau)$. $r(\tau)$ is used for sample correlation coefficients with $\rho(\tau)$ designates population coefficients. Soper (1915) has derived the distribution of sample correlation coefficients with the parameters

$$\bar{r} = \rho \left[1 - \frac{1-\rho^2}{2N} \right] \tag{3.20}$$

and

$$\sigma(\rho) = \frac{1-\rho^2}{\sqrt{N-1}} \left[1 + \frac{1+\rho^2}{4N} \right] \tag{3.21}$$

where N is the number of sampling points used in computing the correlation coefficient. For large N it is possible to write

$$\bar{r} = \rho \tag{3.22}$$

and

$$\sigma(\rho) = \frac{1-\rho^2}{\sqrt{N-1}} \tag{3.23}$$

If the population coefficient is unknown, as is usually the case, then a good estimate of the variance is

$$\sigma(r) = \frac{1-r^2}{\sqrt{N-1}} \quad . \tag{3.24}$$

Bartlett (1956) has shown that the variance of a computed correlation coefficient from a time series is related to the complete auto-correlation function by

$$\text{VAR } [r(\tau)] \simeq \frac{1}{T} \int_{-\alpha}^{\alpha} \rho^2(v)dv \tag{3.25}$$

where T is the length of the sample, and the correlation between a pair of auto-correlation coefficients by

$$R[r(\tau), r(\tau+s)] \simeq \frac{\int_{-\alpha}^{\alpha} \rho(v)\rho(v+s)dv}{\int_{-\alpha}^{\alpha} \rho^2(v)dv} \quad . \tag{3.26}$$

From the expression (3.24) for variance it would seem that in order to reduce the variance it would be sufficient to increase the number of scaled ordinates measured from the amplitude function. It would then be possible to make an estimate of the correlation coefficient with zero variance by taking the number of scaling points sufficiently large. This obviously cannot be true; there must exist a number N such that scaling at more than N points does not decrease the variance. This N is called the number of independent points and implies that amplitudes scaled at intervals smaller than $\frac{T}{N}$ are not independent of each other.

The question arises as to what value of N should be used for a certain length of record. Setting the square of Equation (3.24) equal to Equation (3.25)

gives

$$\frac{(1-\rho^2)^2}{N-1} = \frac{1}{T} \int_{-\alpha}^{\alpha} \rho^2(v)\,dv \tag{3.27}$$

and rearranging gives

$$N = \frac{T}{\int_{-\alpha}^{\alpha} \rho^2(v)\,dv} (1-\rho^2)^2 + 1 \quad . \tag{3.28}$$

The maximum value of N occurs at ρ=o and then

$$N = \frac{T}{\int_{-\alpha}^{\alpha} \rho^2(v)\,dv} + 1 \quad . \tag{3.29}$$

Equation (3.29) is the maximum number of points for independent amplitude measurements.

It is possible to determine the value of N for specific forms of correlation function. For $\rho(v) = \exp\left\{-\frac{v^2}{2b^2}\right\}$, namely a Gaussian correlation function, where b is defined by the relationship $\rho(b) = 0.61$ gives

$$N = \frac{T}{\sqrt{\pi}\, b} \quad . \tag{3.30}$$

Thus the number of independent points is easily calculated from the time structure of the auto-correlation function. Since N must be known to calculate the correlation function, an auxiliary form of Equation (3.30) must be derived. Bowhill (1956) has shown that the average fading period T_2 defined by

$$T_2 = \frac{T}{\text{no. of maxima of the amplitude in time T}}$$

is given for a Gaussian auto-correlogram, by

$$T_2 = 3.63\ b \tag{3.31}$$

b is measured in minutes. Substituting Equation (3.31) into Equation (3.30) gives

$$N = \frac{T}{\sqrt{\pi}} \cdot \frac{3,63}{T_2} = \frac{T}{\sqrt{\pi}} \cdot \frac{3.63}{T} \cdot \text{(no. of maxima in T)}$$

and finally N = ...(no. of maxima in T) ≃ 2(no. of maxima). This relation, which is identical with the sampling theorem of information theory, shows that a record should be scaled at a number of ordinates at least twice the number of maxima occurring on the record. Scaling at closer intervals gives no increase in accuracy in the estimate of the correlation coefficient, while scaling at wider intervals increases the variance of the distribution.

The effect of varying the sampling interval for a given sample on the computer correlation coefficients is illustrated in Figure 3.3. No appreciable difference is observed when the scaling interval is changed from 1 sec to 0.25 sec. In practice an extra factor of two is included as the factor of safety and the number of scaling points is set at >2N. The scaling interval is chosen by observing the correlograms for different samples and finally decided to be 1 second.

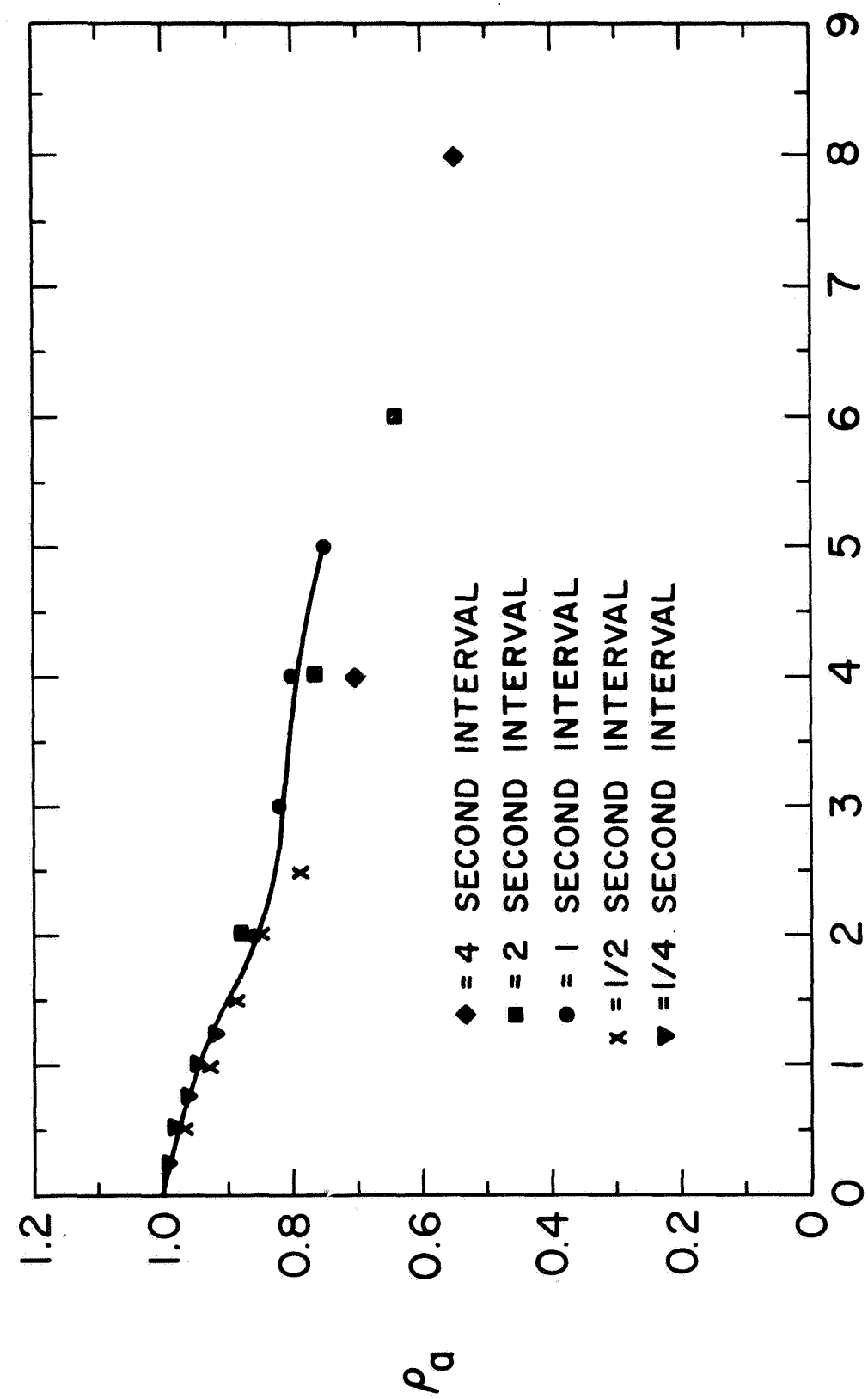

Figure 3.3 Auto-correlograms for different sampling intervals.

4. EXPERIMENTAL RESULTS

The experimental results presented in this chapter pertain to the observations made at the Aeronomy Field Station of the University of Illinois during May and June 1967. The readings were taken in the daytime starting from 0845 hours in the morning to 1945 hours in the afternoon. Fading records at the three stations were simultaneously taken at an interval of one hour and each record is of 15-minute duration. The choice of this duration conforms with the assumption that the drift velocity and other parameters do not change appreciably during this time and this record is sufficiently long to give an adequate population for statistical studies.

The experimental results are divided into two main subjects: the movements of the diffraction pattern observed over the ground and the spatial properties of the pattern. The movements comprise of drift and random velocities while the spatial properties are the axial ratio, tilt angle and structure size of the spatial correlation ellipses. A harmonic analysis of the N-S and E-W components of the drift velocities are carried out and the semidiurnal components are evaluated from the hourly mean values. Emphasis is placed on the diurnal variations of the above parameters and the results are grouped on a monthly basis. The results presented in this chapter were obtained from a total of 90 15-minute samples. The monthly distribution of the number of samples is given in Table 4.1. All the results were computed by the 7094 computer of the University of Illinois and are presented in graphic forms.

4.1 Drift Velocities

The true drift velocity, V_D, was determined for each 15-minute sample using the procedure described in Chapter 3. Drift velocities were found to vary in

Table 4.1 Solar Semidiurnal Component of Drift Velocity

Month	No. of Samples	N-S Component		E-W Component	
		V m/s	θ_o degrees	V m/s	θ_o degrees
May	38	29.5	90	20	82
June	52	16.5	32	20.6	13

magnitude and in direction from sample to sample. The variation of the drift velocities throughout the day are illustrated by the polar plot of this quantity determined from the particular days of May 4, May 19, June 9 and June 20, 1967, in Figures 4.1 - 4.4. The lines shown are obtained by joining the tips of the velocity vectors.

It is found to move in a completely random fashion and the clockwise rotation of the velocity vector cannot be predicted. The reversal of the direction of the velocities can be seen from the Figures 4.5 to 4.8 which are plots of the N-S and E-W components of the drift velocities for these particular days. The velocities directed toward north are considered positive and those toward south are considered negative. Similarly for the E-W component, those velocities toward east are taken as positive and those toward west are negative.

As a consequence of the random nature of the observed values for particular days it was decided to obtain the hourly mean values of the drift velocities from the total number of observations. Histograms of the variations of the drift velocities, random velocities, and for the spatial properties of the correlation ellipse, the axial ration, structure size and tilt angle are obtained. The hourly mean values of the E-W and N-S components are also plotted.

The theory of the atmospheric oscillations predicts diurnal movements in the upper atmosphere due to solar heating effects and a solar semidiurnal movement due to solar and lunar tidal effects (Mitra, 1952). Therefore, in studying atmospheric movements, it is desirable to search for the presence of both the diurnal and semidiurnal harmonic components. However, since the present study is limited to daytime observations only, the semidiurnal component could be studied by applying Fourier analysis.

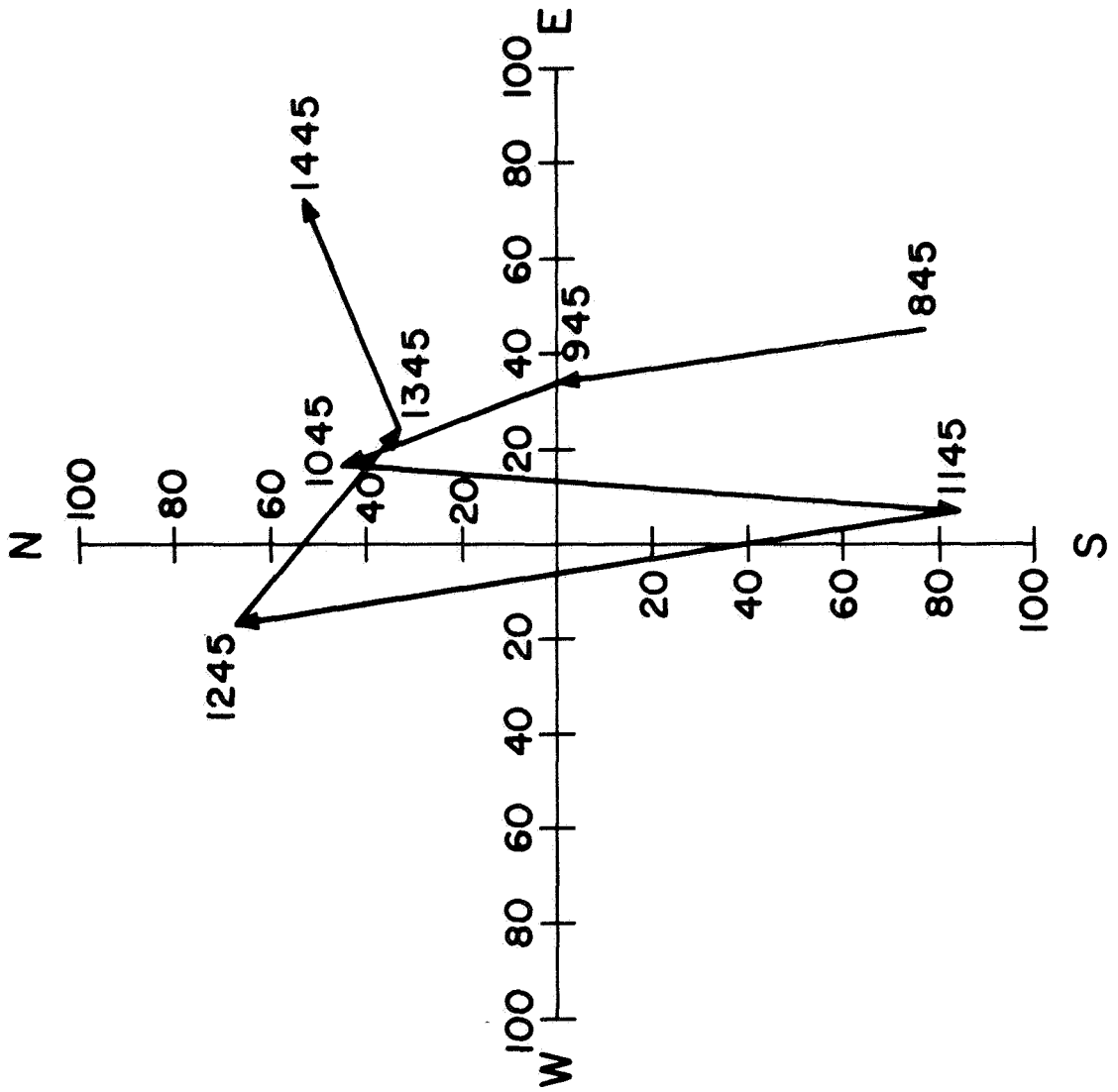

Figure 4.1 Hourly variation of drift velocity, May 4, 1967.

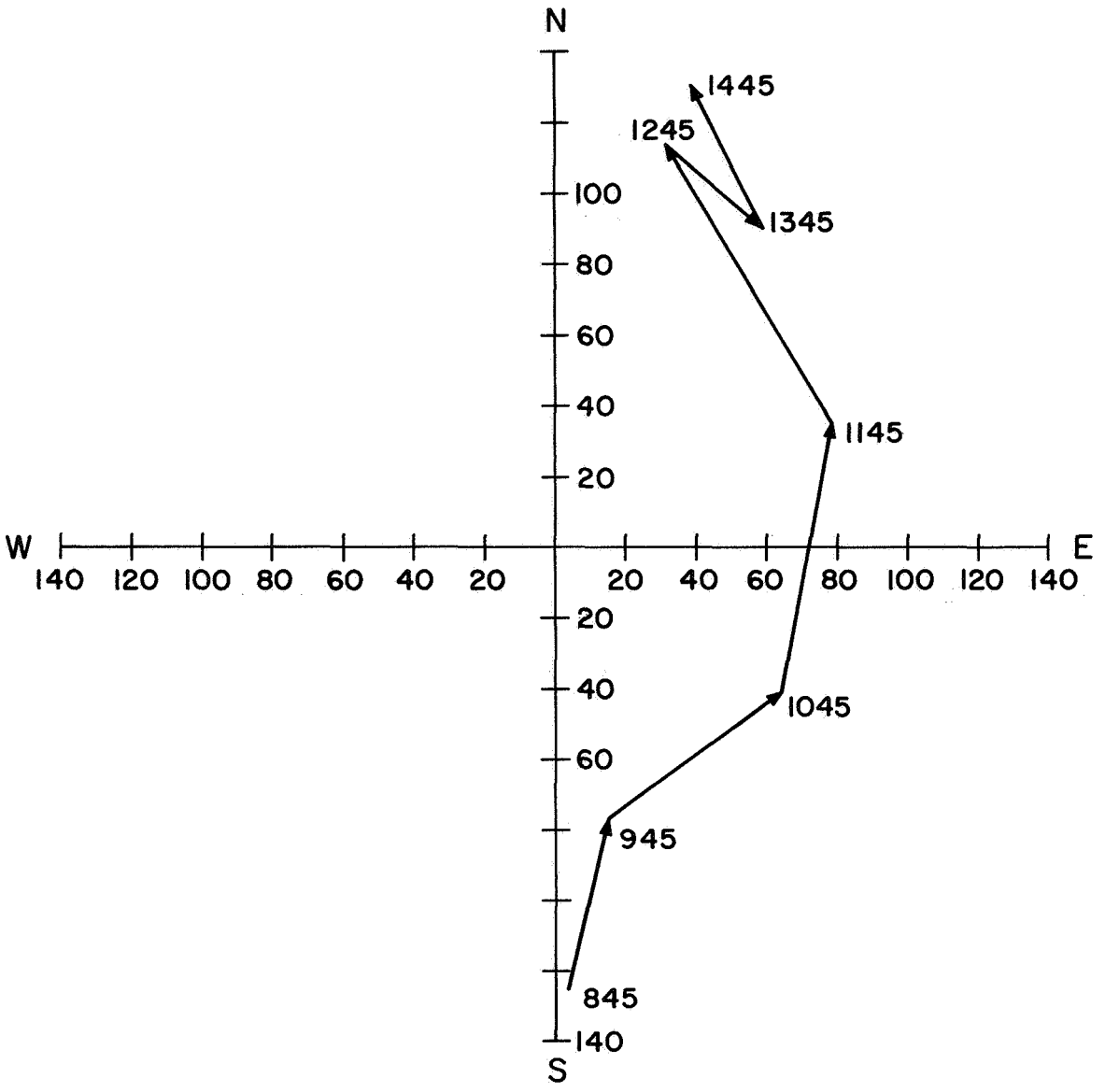

Figure 4.2 Hourly variation of drift velocity, May 19, 1967

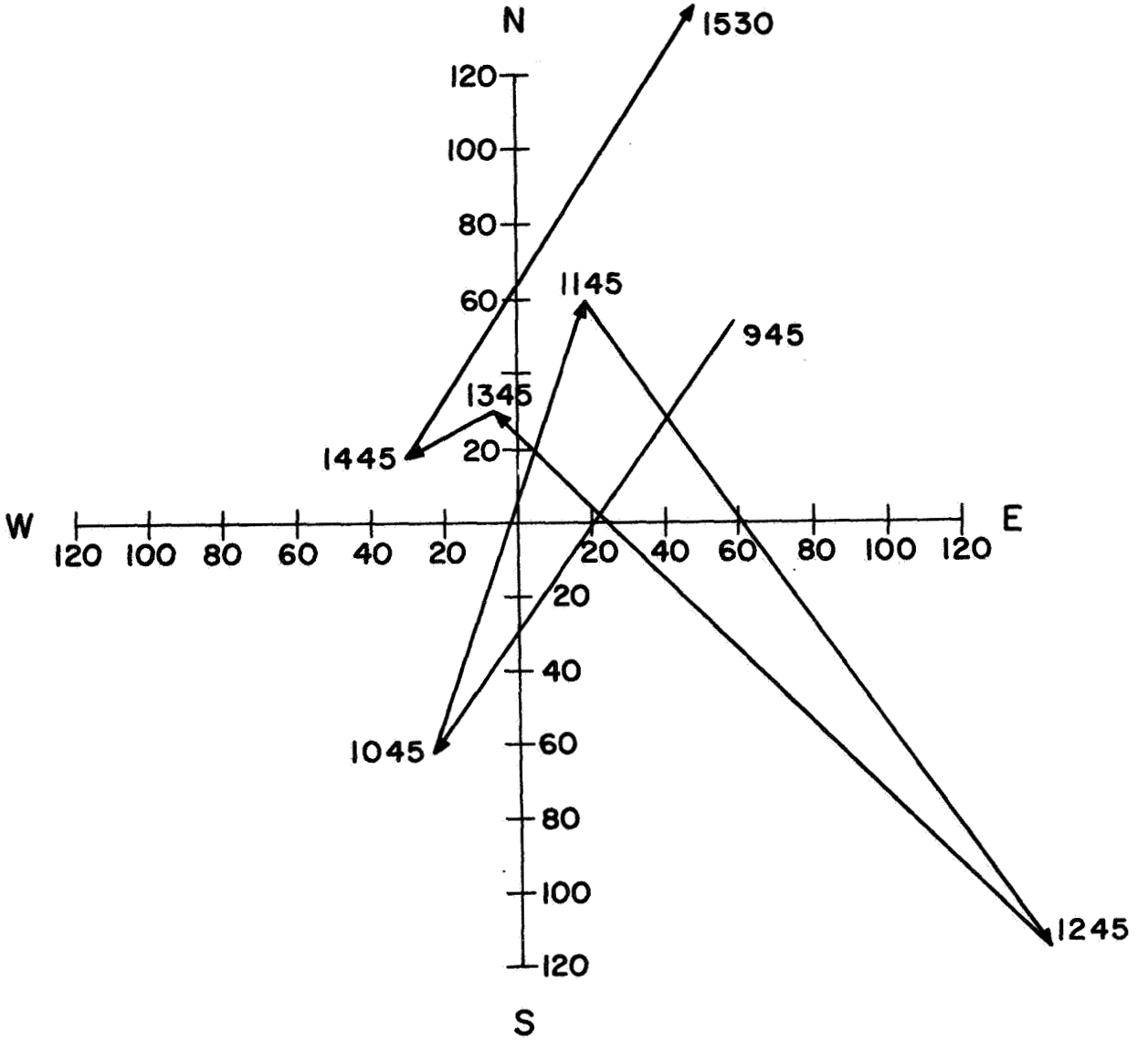

Figure 4.3 Hourly variation of drift velocity, June 9, 1967.

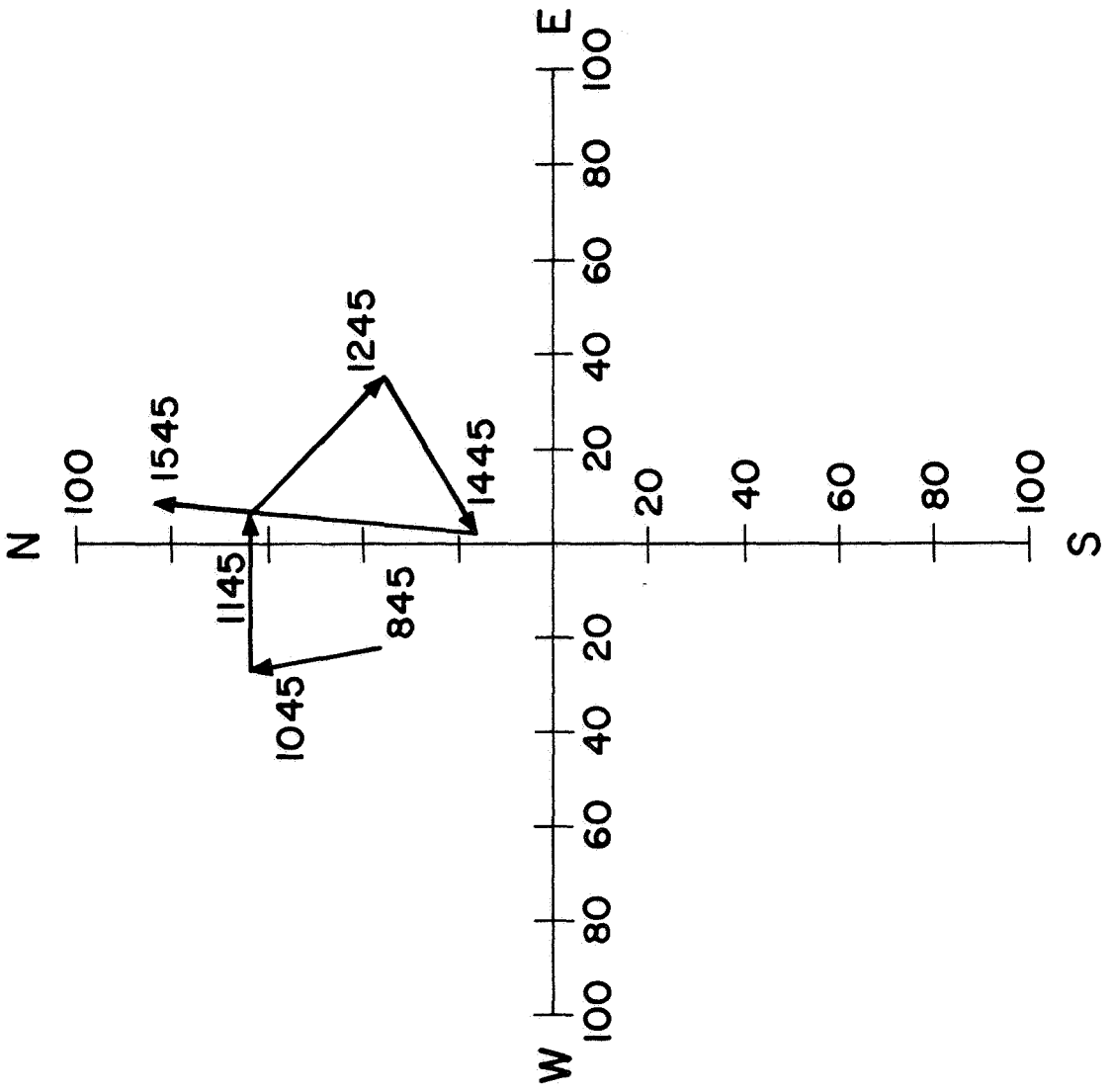

Figure 4.4 Hourly variation of drift velocity, June 20, 1967.

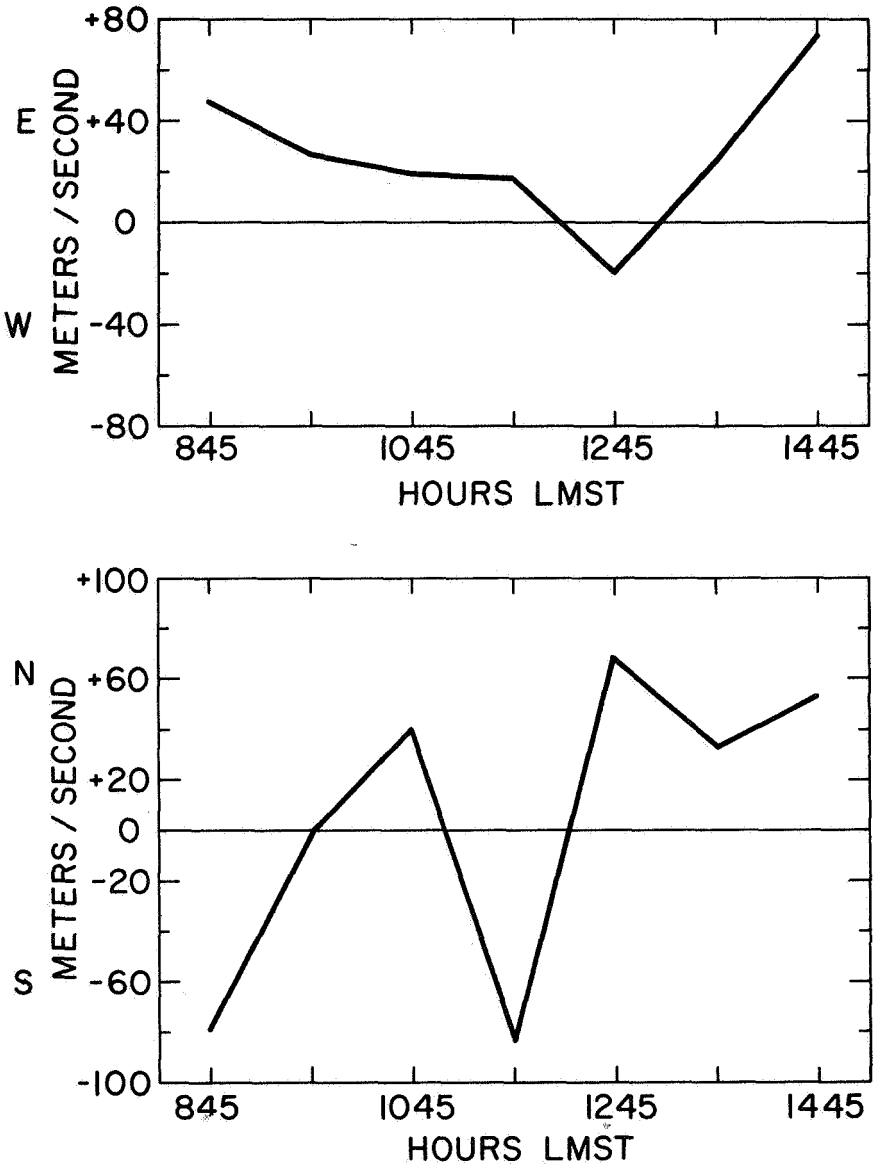

Figure 4.5 Hourly variation of N-S and E-W component of drift velocity, May 4, 1967.

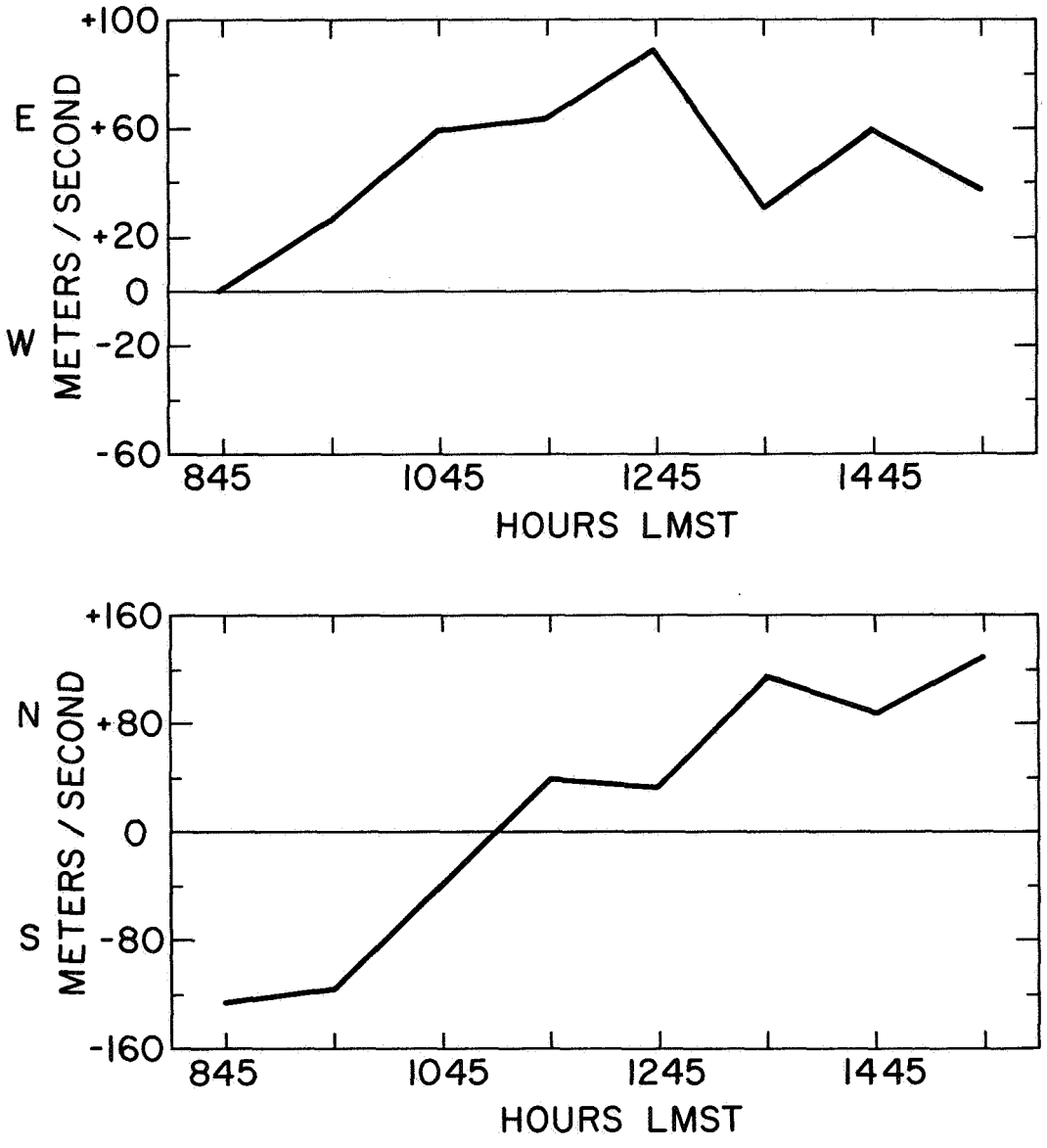

Figure 4.6 Hourly variation of N-S and E-W component of drift velocity, May 19, 1967.

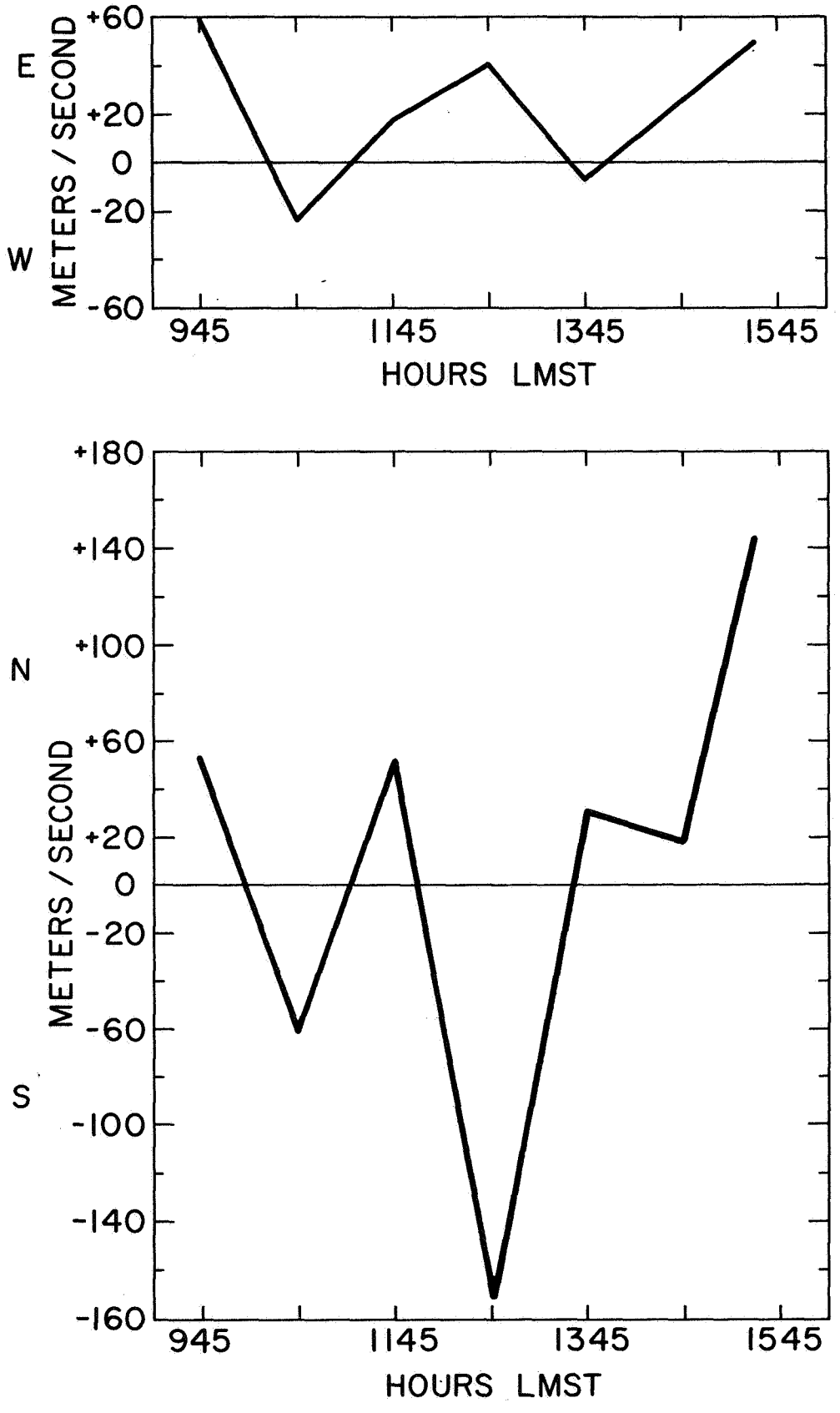

Figure 4.7 Hourly variation of N-S and E-W component of drift velocity, June 9, 1967.

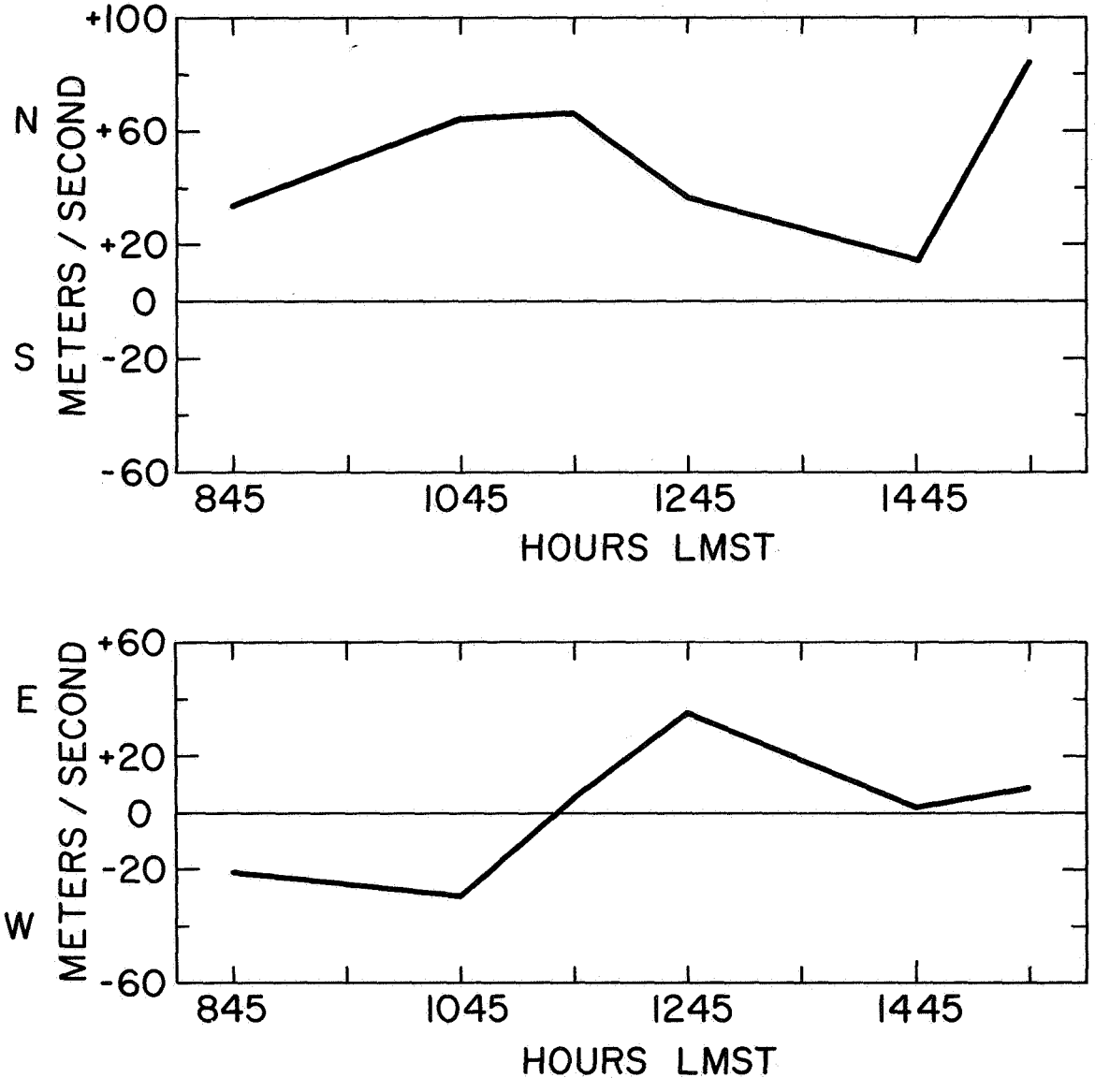

Figure 4.8 Hourly variation of N-S and E-W component of drift velocity, June 20, 1967.

We shall now describe the results obtained by the hourly mean values of the observation and the harmonic analysis results in the following sections.

4.2 Velocities

Figures 4.9 and 4.10 depict the histograms of the drift velocity and random velocity, respectively, obtained for the months of May and June 1967. The median values are chosen as an index instead of the mean value because the former is a better measure of central tendency than the mean, in the presence of a few abnormal values either extremely large or small.

The hourly variation of the E-W and N-S components for the months of May and June 1967 computed as mean of all the hourly values are shown in Figures 4.11 to 4.14. The positive and negative signs in these diagrams were discussed earlier.

4.3 Spatial Properties of the Diffraction Pattern

The diffraction patterns on the ground were assumed to be statistically elliptical and they were represented by spatial correlation ellipses as described in Chapter 3. The spatial properties of the diffraction pattern (the axial ratio S, tilt angle ψ and structure size d) presented in this section are those of the correlation ellipses. These three parameters are studied in the same manner as the drift and random velocities and their histograms are plotted in Figures 4.15, 4.16 and 4.17, respectively. Their median values also are shown in the diagrams. Since the structure size d is different in the three directions of the receiving antennas, the mean value of the three sizes are taken. The tilt angles refer to the angle made by the semimajor axis with the W-E direction and can be seen to lie mostly in the N-E quadrant within 40 to 50 degrees. The structure size lies mostly around 200 meters, as can be seen from Figure 4.17 and the axial ratio centers around a value of two as is evident from Figure 4.15.

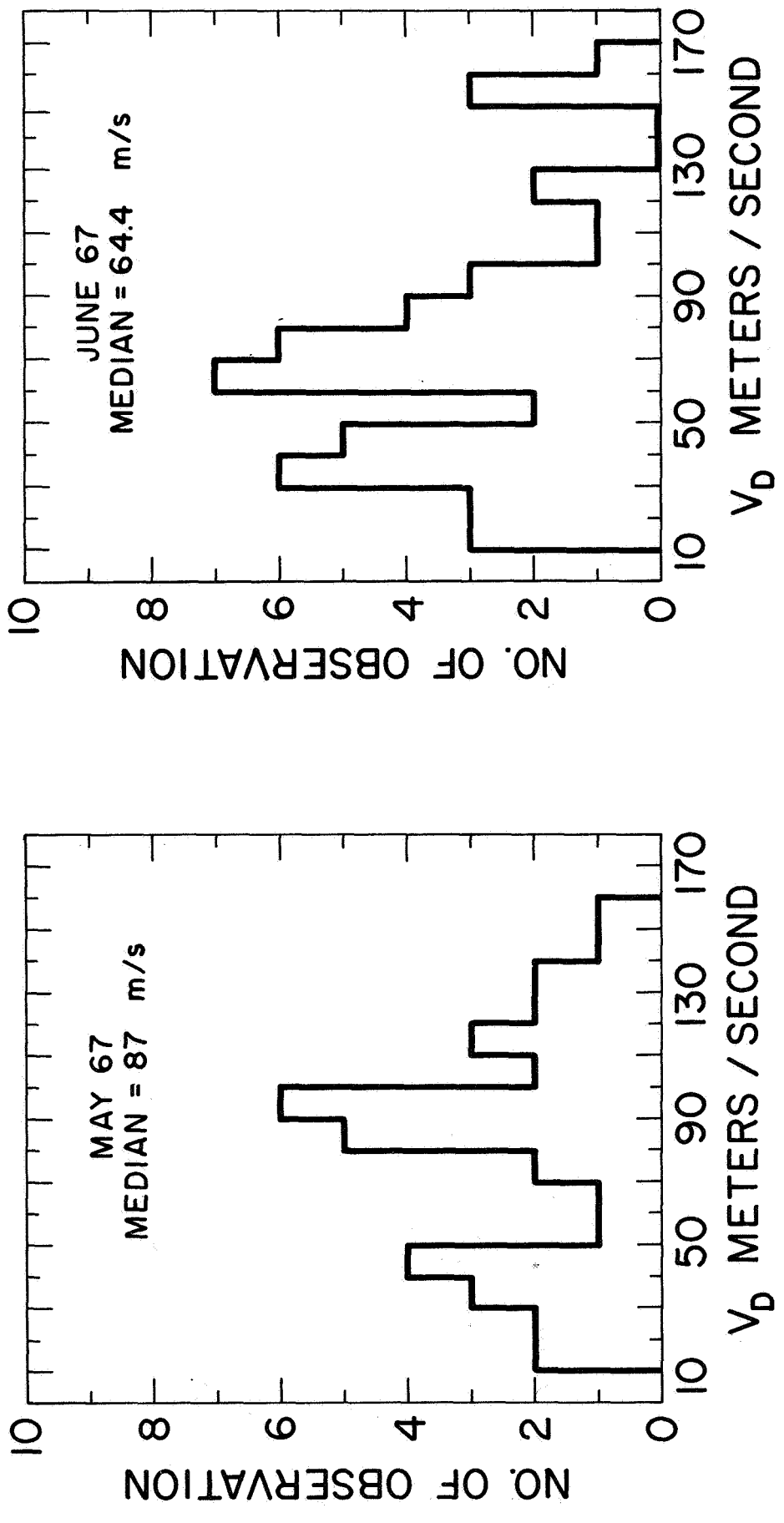

Figure 4.9 Distribution of drift velocity, May and June 1967.

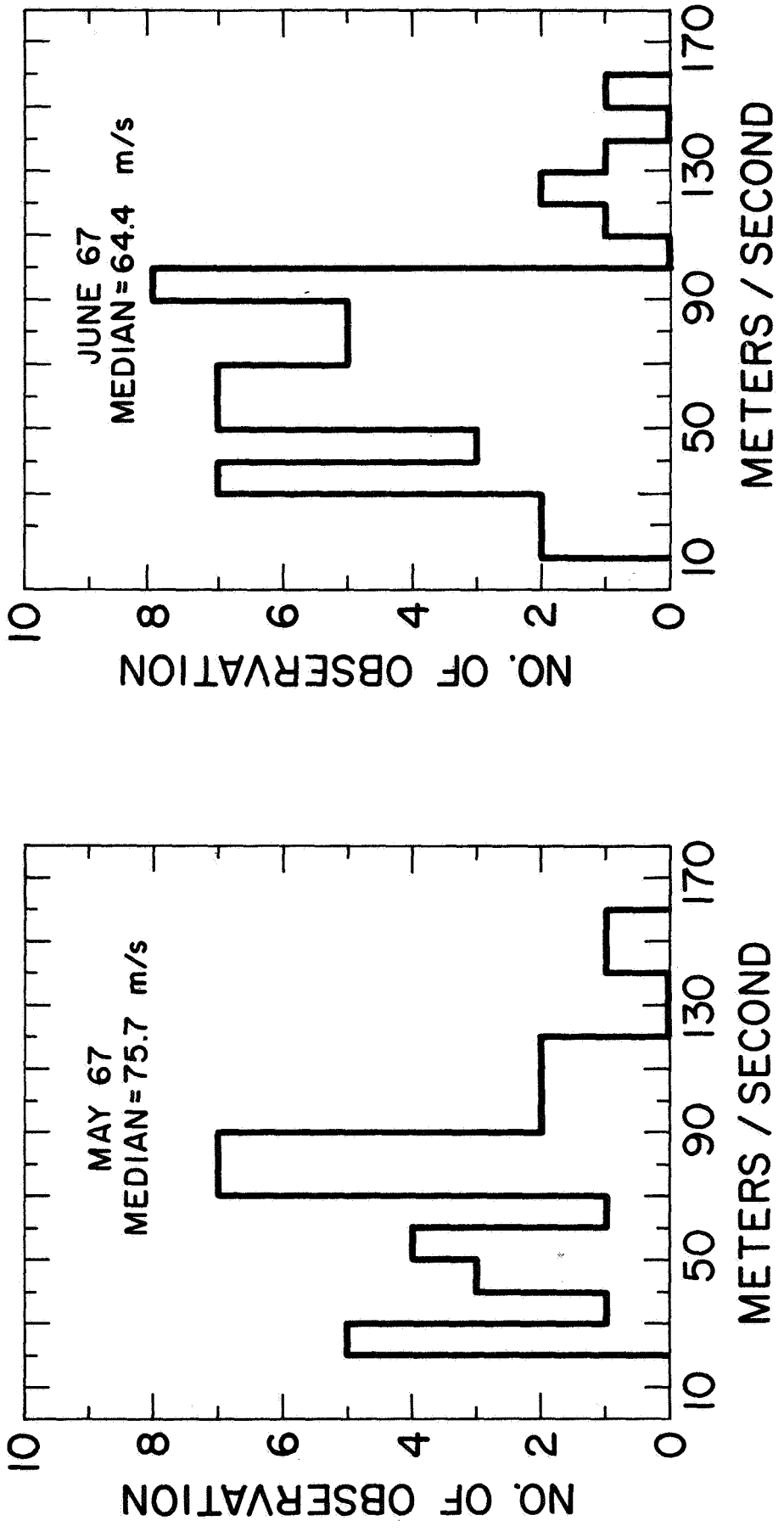

Figure 4.10 Distribution of random velocity, May and June 1967.

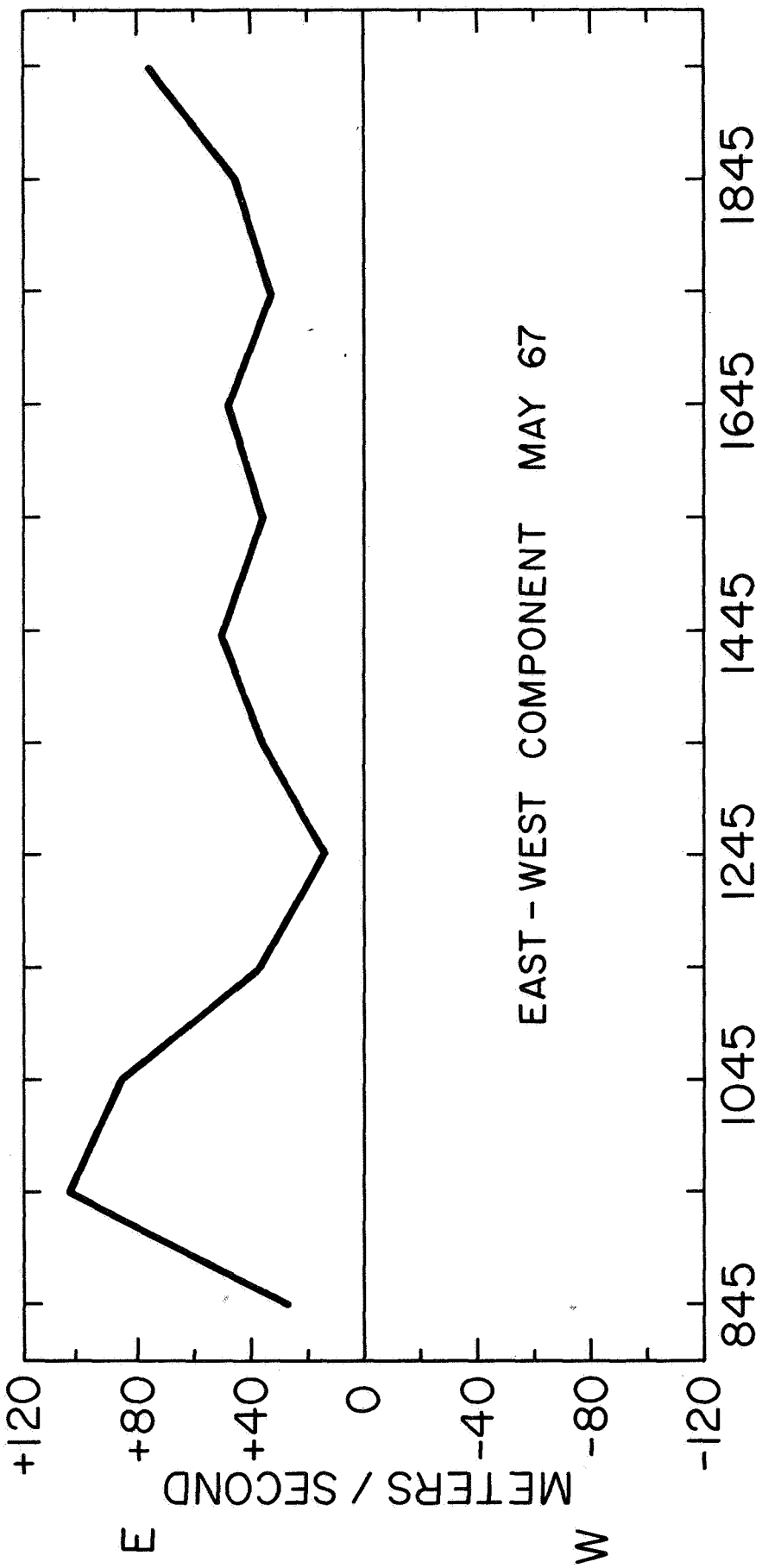

Figure 4.11 Mean hourly variation of E-W component of drift velocity, May 1967.

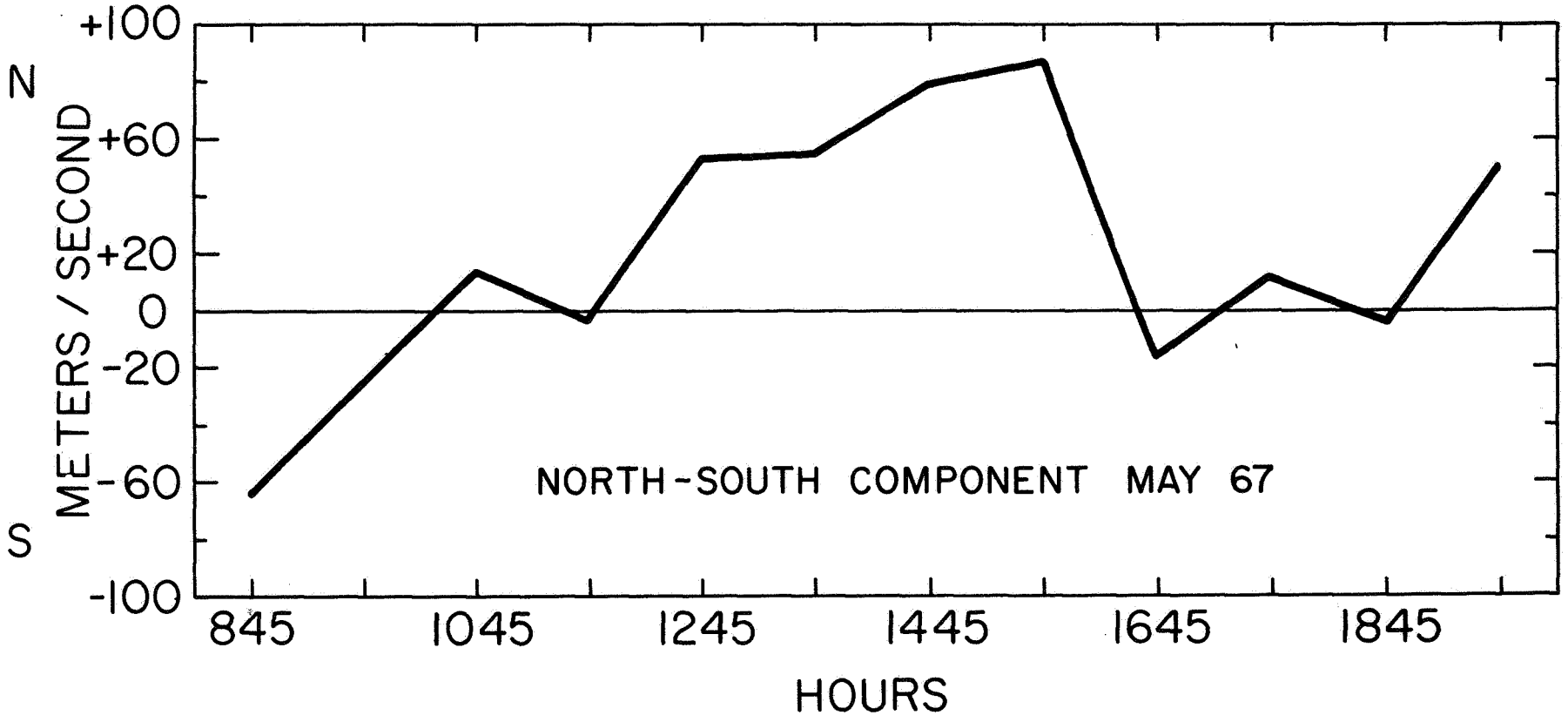

Figure 4.12 Mean hourly variation of N-S component of drift velocity, May 1967.

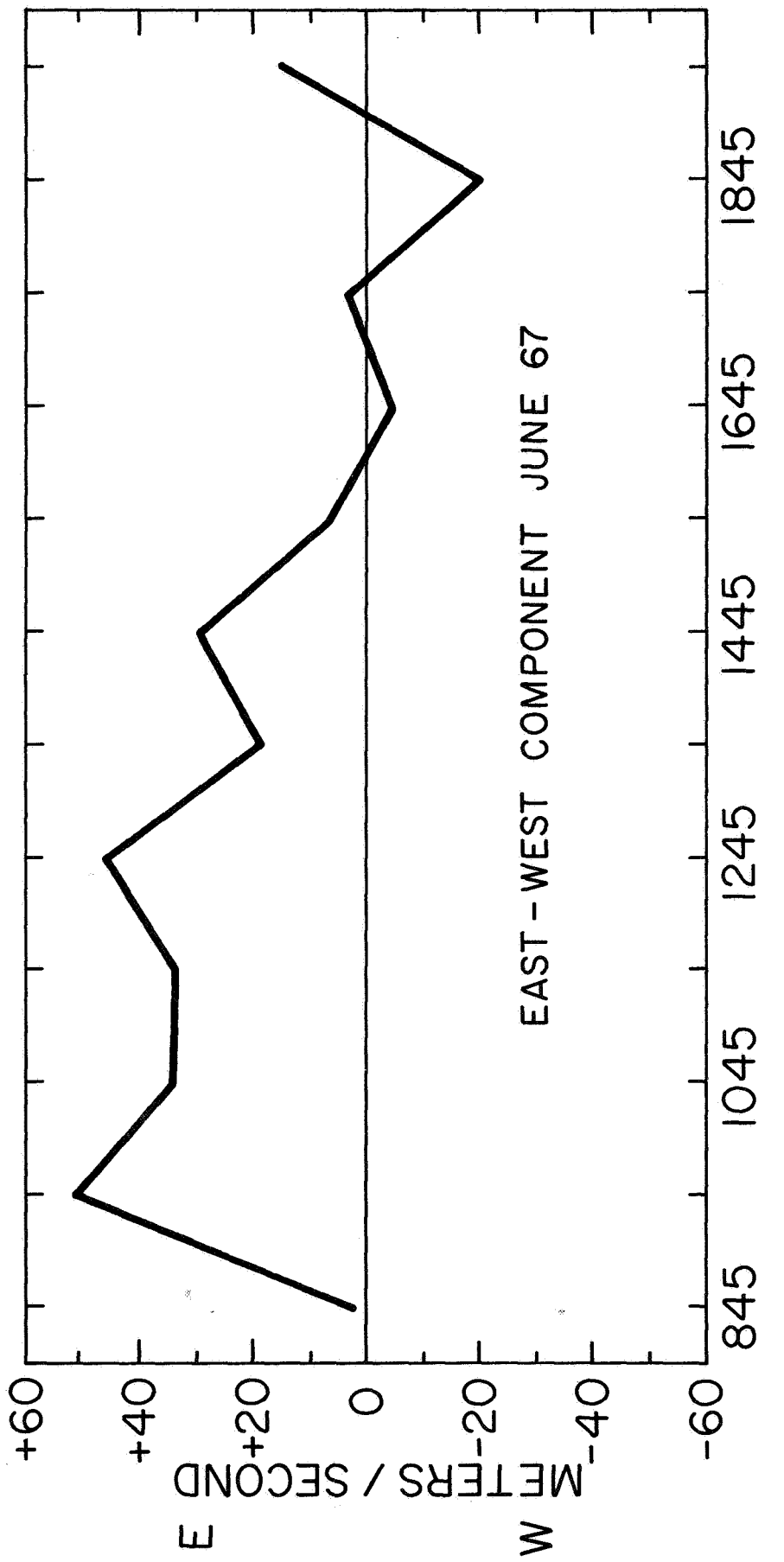

Figure 4.13 Mean hourly variation of E-W component of drift velocity, June 1967.

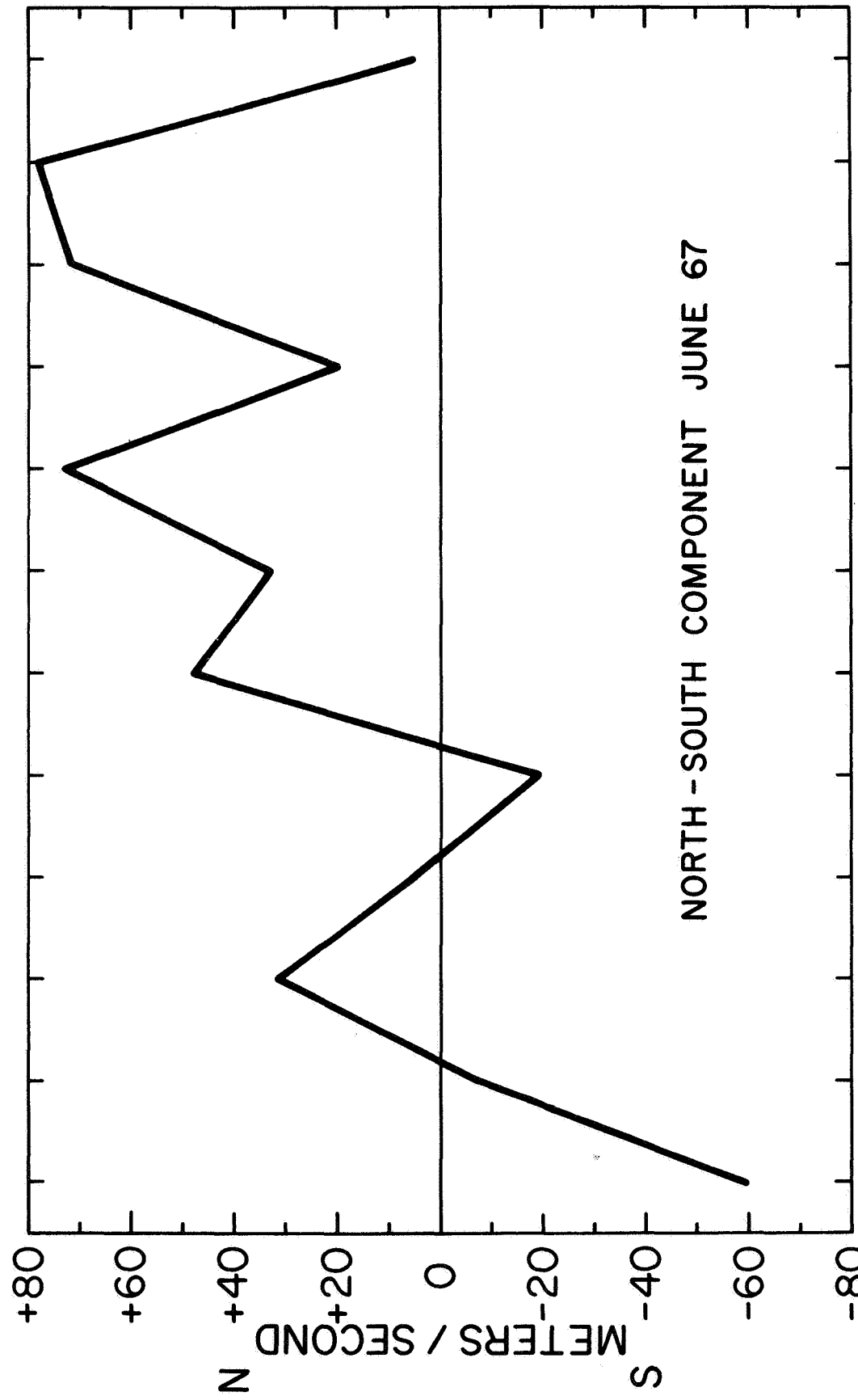

Figure 4.14 Mean hourly variation of N-S component of drift velocity, June 1967.

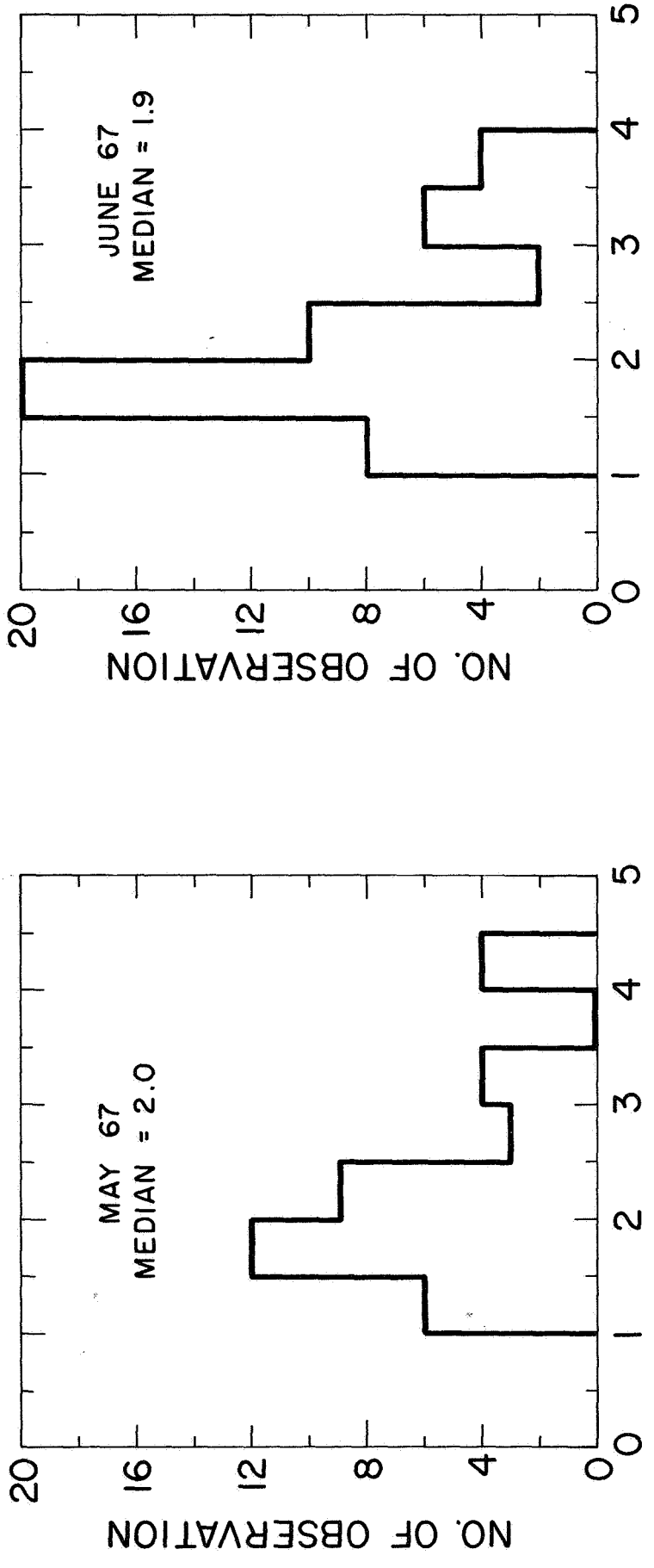

Figure 4.15 Distribution of axial ratio S, May and June 1967.

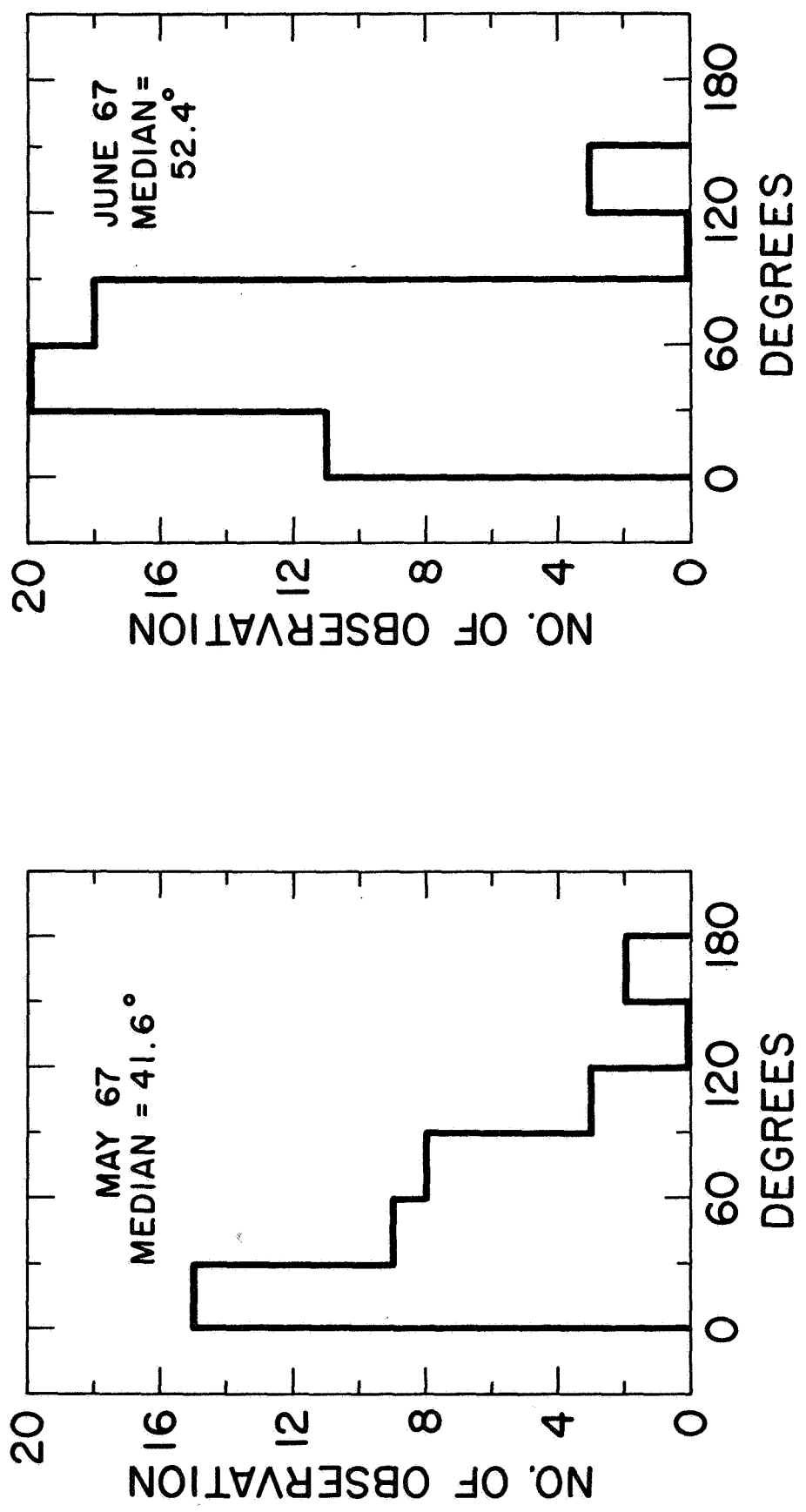

Figure 4.16 Distribution of tilt angle ψ, May and June 1967.

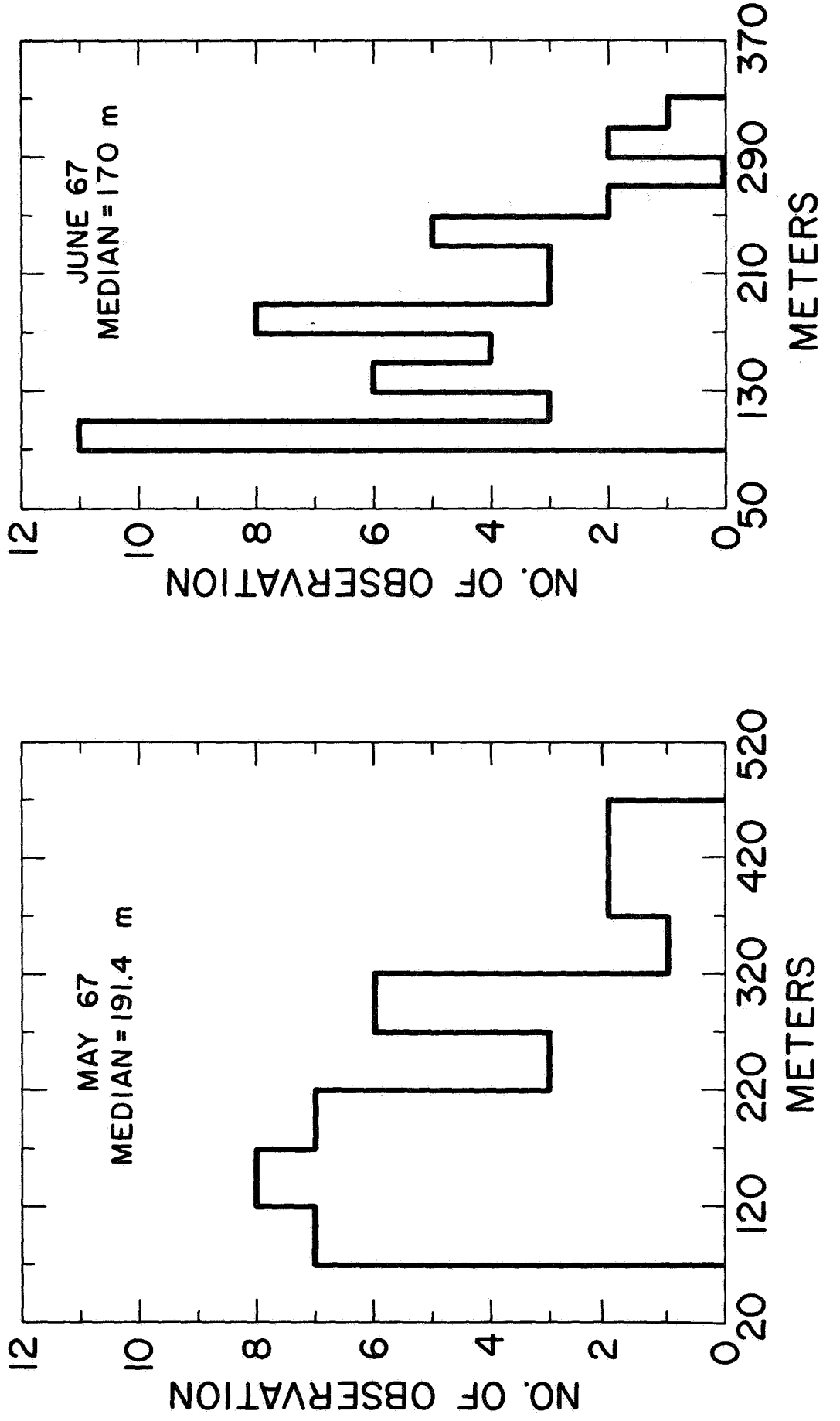

Figure 4.17 Distribution of structure size of the irregularities d, May and June 1967.

4.4 Semidiurnal Components

By carrying out the Fourier analysis for the N-S and E-W components for the months of May and June as shown in Figures 4.11 to 4.14, the semidiurnal components for these months are obtained. Table 4.1 contains the magnitude V and the phase angle θ_o of the semidiurnal components which were expressed in the following general form

$$V \sin (2\theta + \theta_o)$$

where θ is the hour angle, increasing by 15 degrees per hour. In Figures 4.18 and 4.19 the monthly semidiurnal components are given in polar plot for the months of May and June. The number attached to the points indicate the times of commencement of each hour and the scales are in m/s. It is seen that the semidiurnal components rotate anticlockwise in the case of May 1967 and clockwise in the case of June 1967 and a 180 degree phase lag between the two diagrams are observed. Table 4.2 presents the median values for all parameters.

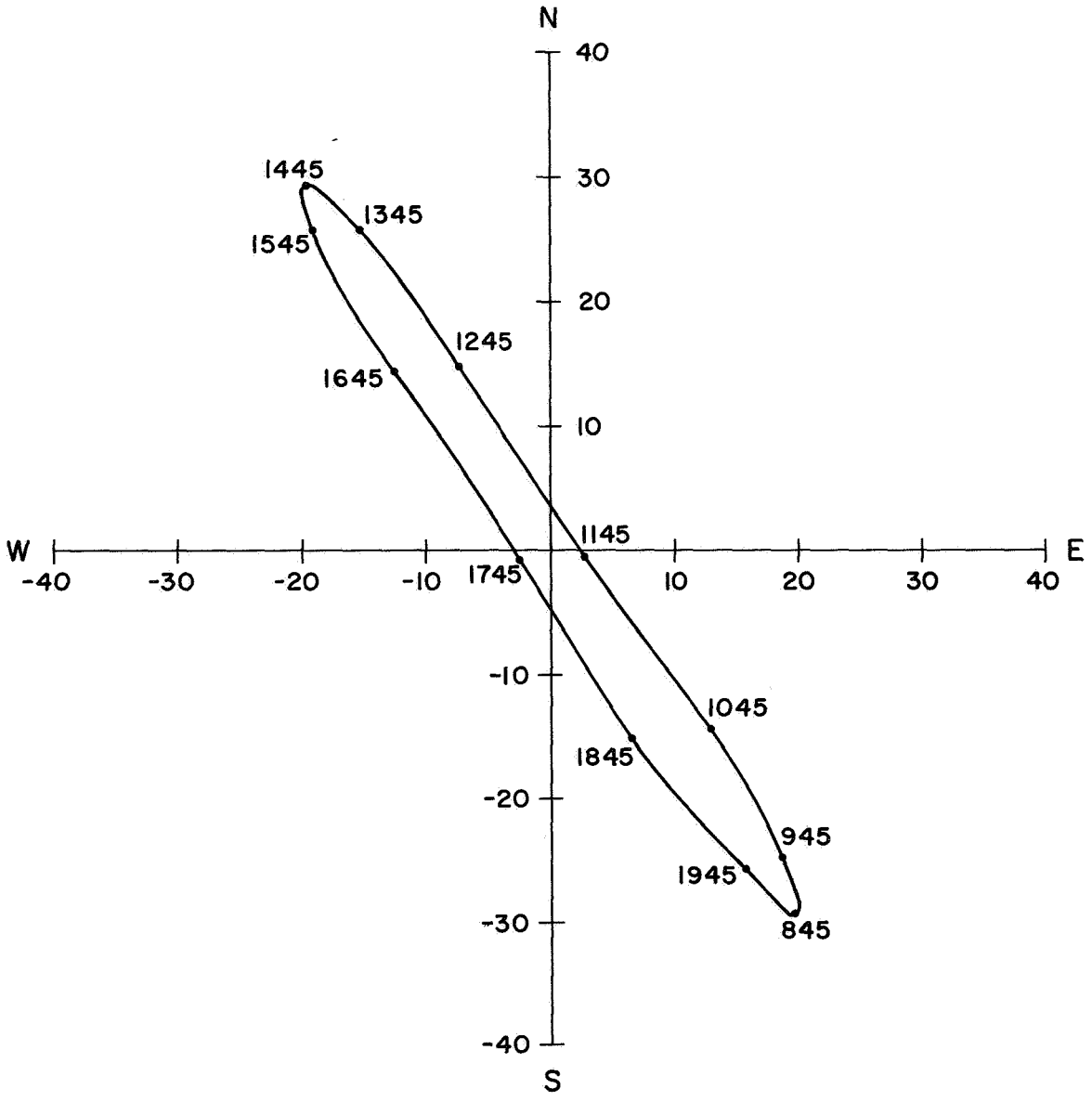

Figure 4.18 Polar plot of semidiurnal component of drift velocity, May 1967.

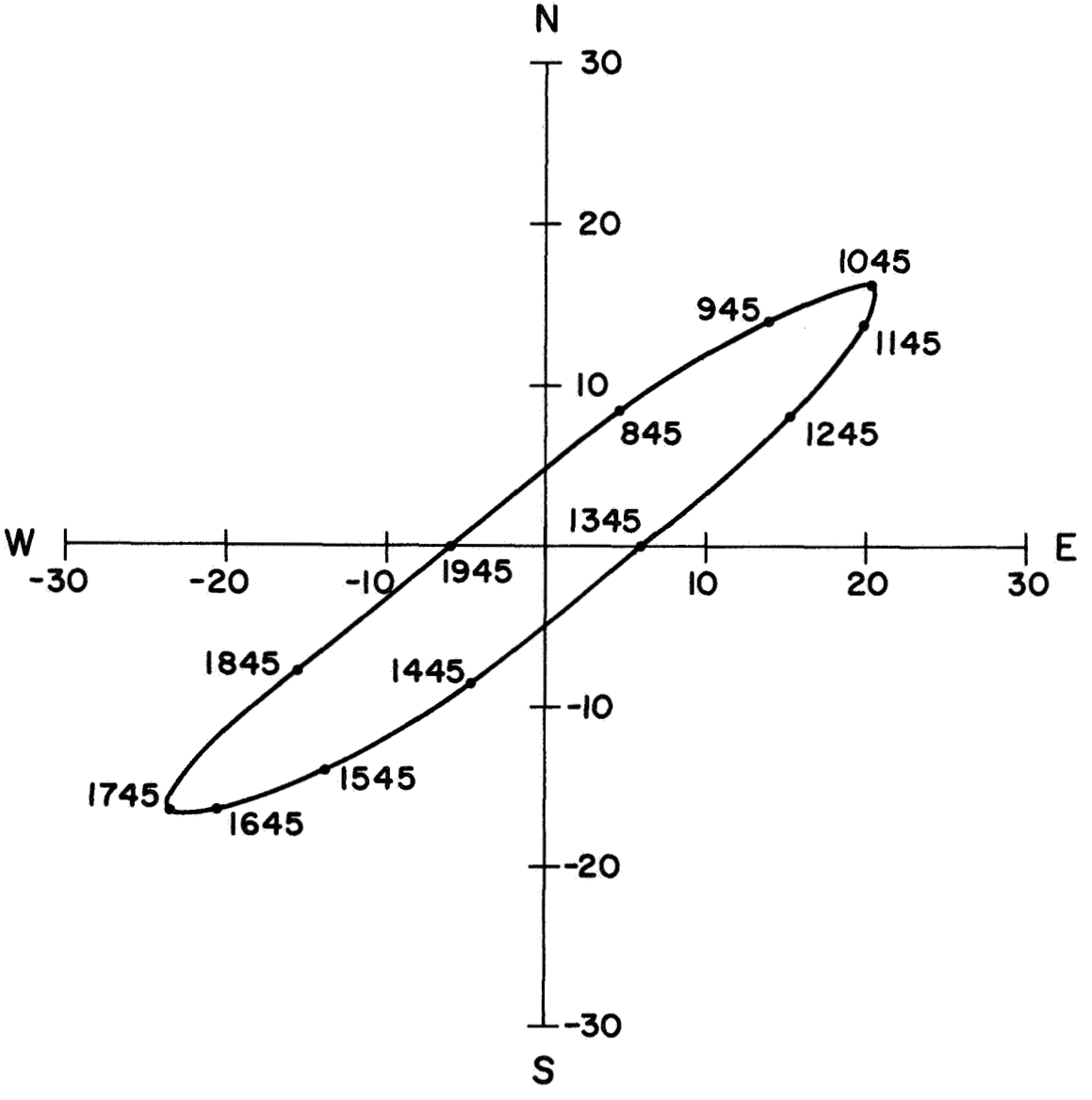

Figure 4.19 Polar plot of semidiurnal component of drift velocity, June 1967.

Table 4.2 Median Values of Velocity and Anisotropy Parameters

Month	V_D m/s	V_R m/s	s	d meter	ψ degrees North of East
May	87	75.7	2.0	191.4	41.6
June	64.4	64.4	1.9	170	52.4

5. SUMMARY AND CONCLUSION

An investigation of statistical properties of the apparent horizontal ionospheric movements was carried out for the lower regions of the ionosphere using three receiver techniques. The amplitude fading observed on the ground at three locations separated approximately one wavelength corresponding to the frequency of observations was taken and subjected to correlation analysis by the standard methods and the parameters of drift velocity, random velocity and spatial properties of the correlation ellipse (axial ratio, tilt angle and structure size of the irregularities) are determined.

The results agree with those obtained by other workers in this field. The median drift velocities are also of the same order. The axial ratio of the correlation ellipse is of the order of 2, and the major axis being oriented in the N-E direction. The structure size of the irregularities is of the order of 200 m; the rather large value of the axial ratio suggest the necessity of anisotropy corrections to be applied to the parameters experimentally obtained. The drift velocities of the individual days do not show the orderly clockwise rotation observed by other workers; but the number of observations is not adequate to reach a firm conclusion in this matter.

Harmonic analysis was applied to the E-W and N-S components of drift velocities obtained; a clockwise rotation of the semidiurnal component was found in one month, and an anticlockwise rotation in the other month. Moreover, a 180 degree phase difference was found between the two sets of observations.

It was felt in analyzing the data that some device should be developed in order to read automatically the large amount of data necessary in such an analysis, by punched paper tape or some other electronic means. Based on this

method of analysis, a three-dimensional picture of the drift velocities in the ionosphere might be investigated by applying different closely-spaced frequencies for probing the ionospheric layers at different levels.

REFERENCES

Bartlett, M. S. (1956), Stochastic Processes, Cambridge University Press, Cambridge.

Bowhill, S. A. (1956), The fading of radio waves of frequencies between 16 and 2400 kc/s, J. Atmosph. Terrest. Phys. 8, 120-145.

Brennan, D. G. (1960), Statistical Methods in Radio Wave Propagation, Pergamon Press, New York.

Briggs, B. H., G. J. Phillips and D. H. Shinn (1950), The analysis of observations on spaced receivers of the fading of radio signals, Proc. Phys. Soc. B, 63, 106-121.

Briggs, B. H. and M. Spencer, (1954), Horizontal movements in the ionosphere, The Phys. Soc. Rept. Progress in Phys. 17, 245-280.

Briggs, B. H. and E. S. Page (1954), An empirical study of random functions which arise in the interpretation of ionospheric movements, Rept. of Phys. Soc. Conf. on Physics of the Ionosphere, 119-122.

Henry, G. W. Jr. (1966), Instrumentation and preliminary results from shipboard measurements of vertical incidence ionospheric absorption, University of Illinois Aeronomy Report No. 13.

Landee, R. W., D. C. Davis and A. P. Albrecht (1957), Electronic Designers Handbook, McGraw Hill Book Co., New York.

Lee, H. S. (1962), A statistical study of apparent horizontal ionosphere movements using 300 kc/s radio waves, Penn. State Scientific Rept. No. 170.

Mitra, S. K. (1952), The Upper Atmosphere (Second edition), The Royal Asiatic Society, Calcutta, India.

Mitra, S. N. (1949), A radio method of measuring winds in the ionosphere, Proc. IEE 96, 441-446.

Phillips, G. J. and M. Spencer (1955), The effects of anisometric amplitude patterns in the measurement of ionospheric drifts, Proc. Phys. Soc. 68, 481-492.

Pütter, P. S. (1954), Messung des ionospherenwindes aus der wanderungsgeschwindigkeit eines zustandes (Z.B. Echo-Feld Stärke) längs der Erdoberfläche, Rept. of Phys. Soc. Conf. on Physics of the Ionosphere, 191-201.

Ratcliffe, J. A. and J. L. Pawsey (1933), A study of the intensity variations of downcoming wireless waves, Proc. Camb. Soc. 29, 301-318.

Soper, H. E. (1915), Biometrica 11, 328.